A study on the graphite fluoride cathode in nonaqueous lithium cell(Dissertation_全文)

AUTHOR(S):

Hagiwara, Rika

A STUDY ON THE GRAPHITE FLUORIDE CATHODE IN NONAQUEOUS LITHIUM CELL

1985

RIKA HAGIWARA

A STUDY ON THE GRAPHITE FLUORIDE CATHODE IN NONAQUEOUS LITHIUM CELL

1985

RIKA HAGIWARA

PREFACE

The study presented here has been carried out under the direction of Professor Nobuatsu Watanabe in his laboratory at Kyoto University.

It was about fifteen years ago that lithium-graphite fluoride battery was proposed as a primary cell by Watanabe and Fukuda. Several types of miniature batteries have been already commercialized. However, the fundamental works on the discharge reaction, kinetics and improvement of discharge characteristics of graphite fluoride cathodes, have not yet been done enough.

The purpose of this work is to elucidate the discharge reaction and kinetics of lithium-graphite fluoride cell and to improve the discharge characteristics of graphite fluoride cathode. The author wishes that the present work may provide a useful groundwork for the further study on graphite fluoride.

The author is greatly indebted to Professor Nobuatsu Watanabe for his kind encouragement, valuable suggestions and discussions throughout the work.

The author would like to express his sincere thanks to Assistant Dr. Tsuyoshi Nakajima for his stimulating discussion and a considerable number of suggestions.

Grateful acknowledgment is made to Assistant Professor Kohichiro Nakanishi and Assistant Dr. Hidekazu Touhara for their helpful advices and discussions during the work.

The author also wishes to thank Messrs. Koji Moriya, Akihiro Mabuchi, Toshiyuki Sakai, Kaoru Nogawa and Kunihiko Ishi for their excellent assistance in the experimental work, and all the members in the laboratory for their kind encouragement and support during the work.

Rika Hagiwara

Department of Industrial Chemistry

Faculty of Engineering
Kyoto University
October, 1985

CONTENTS

GENERAL INTRODUCTION

I. Review of the previous studies

The first synthesis of graphite fluoride was done by Ruff and Bretschneider(1) in 1934. They found that graphite reacted with fluorine gas in the temperature range of 420-460°C to form a gray solid with the F/C ratio of 0.92. Rüdorff et al.(2-6) made a series of studies on graphite fluoride from 1947 to 1959. They confirmed the original observations, reporting that the compounds with compositions ranging from $CF_{0.676}$ to $CF_{0.988}$ were obtained at 410-550°C, the color of which changed from gray to white. An assumed structure of graphite fluoride was also presented by them on the basis of X-ray powder diffraction pattern and IR spectrum.

Watanabe and his coworkers have carried out extensive researches about graphite fluoride,(7-43) beginning from investigations on the notorious 'anode effect' in the production of elemental fluorine or aluminum via molten salt electrolysis using carbon anodes(44-49). They made a series of studies on the mechanism of formation reaction, the crystal structure and physicochemical properties of graphite fluoride, and applied to the cathode material for a primary lithium battery(10). In 1979, a new type of graphite fluoride, $(C_2F)_n$ was found by them(28). Margrave et al. (50-59) also reported the studies on the preparation, crystal structure, heat of formation and thermal decomposition of graphite fluoride from 1965 to 1977. Other several studies were also reported(60-68).

The results of recent studies on graphite fluoride is summarized as follows.

I-1 Synthesis of graphite fluorides

Graphite fluorides are obtained in the form of a para-crystallite by the direct fluorination of carbon materials

at high temperatures. For example, when natural graphite is used as a starting material, $(CF)_n$ is formed around 600°C, while $(C_2F)_n$ is prepared at a lower temperature of 350°-400°C(28). With increasing fluorination temperature, the composition changes from $(C_2F)_n$ to $(CF)_n$ via their mixture, in which $(CF)_n$ content increases with increasing temperature. It is noted that $(C_2F)_n$ is prepared only from a highly crystallized graphite, such as natural graphite or graphitized petroleum coke, at a relatively low temperature.

Reaction time required for the preparation of $(CF)_n$ was several hours, however, that of $(C_2F)_n$ was as long as 2-3 weeks. A new synthetic method of a short time preparation of $(C_2F)_n$ has been developed(36, 40). In this method, ionic graphite intercalation compounds are first formed, and their thermal decomposition provides the exfoliated graphite which is easily fluorinated to give $(C_2F)_n$.

I-2 Crystal structures of graphite fluorides

The carbon layers of graphite fluoride consist of an infinite array of trans-linked cyclohexane chairs without aromatic nature. Both in $(CF)_n$ and $(C_2F)_n$, carbon atom with sp^3-hybridized orbital is covalently bonded to fluorine, differently from the general graphite intercalation compounds with ionic bonds between graphene layer and intercalate. $(CF)_n$ is regarded as a first stage compound, whereas $(C_2F)_n$ is of the second stage. The structures of the monolayers of $(CF)_n$ and $(C_2F)_n$ are shown in Fig 3-2(Chapter 3). The turbostratic stackings of these monolayers are found in general graphite fluorides, however, as an ideal structure, A/A' and AB/B'A' stacking sequences have been proposed for $(CF)_n$ and $(C_2F)_n$, where A' and B' carbon layers are mirror-symmetrical to A and B, respectively(42).

I-3 Physicochemical properties of graphite fluorides

I-3-1 Surface properties(38)

Graphite fluoride, $(CF)_n$ has an extremely low surface energy since the surface is completely covered with fluorine atoms having reasonably low interaction with other atoms or molecules. It is less wettable with liquid than polytetrafluoroethylene(PTFE).

I-3-2 Thermal stability

Graphite fluorides have excellent thermostability. Decomposition temperatures in several kinds of atmospheres are shown in Table 6-1(Chapter 6). Thermal decomposition of graphite fluorides provides fluorocarbon gas with various F/C ratios. The detailed decomposition mechanisms and kinetics have been reported elsewhere(31-33, 61).

I-3-3 Chemical stability

$(CF)_n$ resists attack by strong alkalis or mineral acids. It is decomposed by hydrogen at 450-500°C($\longrightarrow$C + HF), potassium iodide at 360-500°C($\longrightarrow$C + KF + I_2), and potassium carbonate at around 310°C($\longrightarrow$C + KF + CO_2), study of which has provided the value 448.5 $kJmol^{-1}$ for the C-F bond energy(12). Additionally, photolysis of graphite fluoride in some organic solvents has been reported (34).

I-4 Applications of graphite fluorides

I-4-1 Solid lubricant(69-75)

Graphite and molybdenum disulfide are well known as solid lubricants, however they are easily influenced by the working environments. On the other hand, graphite fluoride shows a rather low friction coefficient and long wear life over a wide range of temperature, pressure, and load.

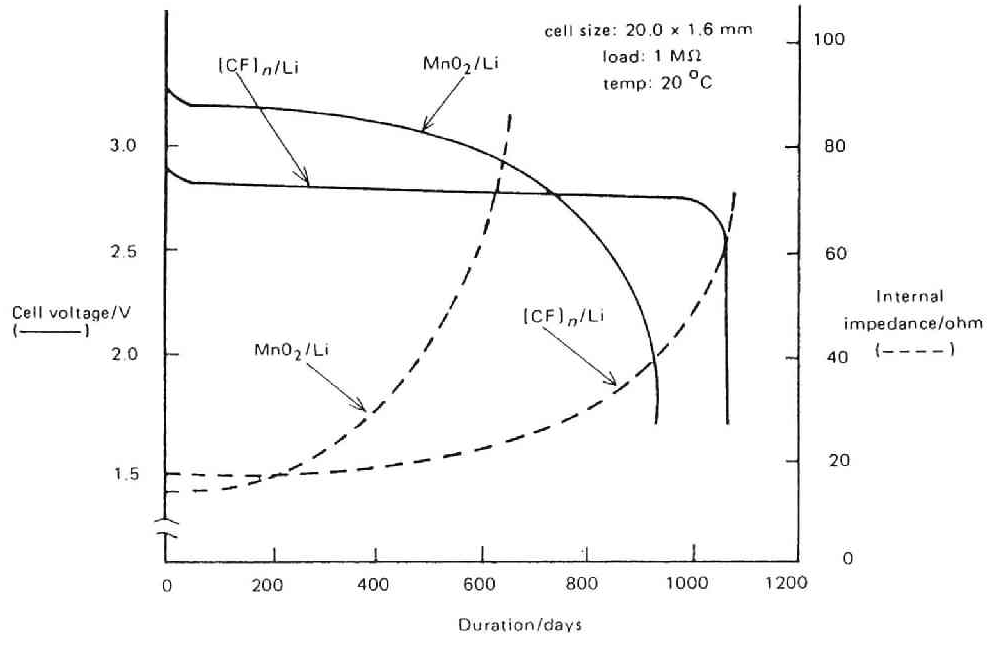

Fig. I-1 Comparison of discharge and impedance characteristics for $(CF)_n$/Li and MnO_2/Li batteries(Ref. 81)

It was revealed in NASA that graphite fluoride is a excellent solid lubricant under a high temperature and pressure(71, 72).

I-4-2 Cathode materials for primary batteries

It was at the beginning of 1970's that application of $(CF)_n$ as a cathode material for a primary lithium battery with organic electrolyte was first proposed(10). In 1970's, several types of Li-$(CF)_n$ batteries were commercialized by Matsushita Electric Co. Ltd.(76-80). This battery has many advantages such as high voltage and energy density, flat discharge potential, discharge capability over a wide range of temperatures, long shelf life, safety and so on. The comparison is made for several miniature primary cells in Fig. I-1(81). Application to the cathode in dry cell

using an aqueous alkaline electrolyte was also proposed(82). Besides $(CF)_n$, it was revealed that a new type of graphite fluoride, $(C_2F)_n$ also had an excellent performance as a cathode mass for a lithium battery(25, 26, 29).

The large difference between a real and theoretical electromotive forces of Li-$(CF)_n$ cell was explained first with "mixed potential theory"(83-85), however, recent investigations(25, 26, 43, 86, 87) suggest that the cell reaction is not the direct formation of LiF and carbon but the graphite intercalation compound.

It has already been found that the Li-$(C_2F)_n$ cell has a higher discharge potential than Li-$(CF)_n$ cell(25), but more detailed electrodics has not yet been clarified.

II. Purpose of the present study

As mentioned above, the most important applications of graphite fluorides is the cathode material for a primary lithium cell. The purpose of the present study is to investigate the electrode reaction, kinetics of Li-graphite fluoride cell and effects of the structure of graphite fluoride on the discharge performance and further to improve the performance of graphite fluoride cathode based on the results obtained.

III. Scope of the present study

Chapter 1 deals with the electrode reactions of two types of graphite fluorides, $(CF)_n$ and $(C_2F)_n$ on the basis of elecrochemical measurements. The effects of the electrolyte solvents on the electrode reaction were investigated using several kinds of organic solvents. A cathode model and formulation of electrode potential are also presented.

Chapter 2 deals with the kinetics of graphite fluoride cathodes. Kinetic parameters were obtained by the aid of transient techniques such as chronopotentiometry and

chronoamperometry.

Chapter 3 is concerned with the relation between the cathode overpotentials and crystallinity of $(CF)_n$ and $(C_2F)_n$. The overpotentials are discussed on the basis of the results obtained by X-ray diffraction, ^{19}F-NMR and ESR measurements.

Chapter 4 deals with the discharge characteristics of $(CF)_n$ and $(C_2F)_n$ prepared via ionic graphite intercalation compound of fluorine in comparison with those of graphite fluorides prepared by direct fluorination method.

Chapter 5 is concerned with the improvement of the discharge performance of graphite fluoride by the reform of the pristine carbon. The reform was made by thermal decomposition of graphite compounds with covalent bonds such as $(C_2F)_n$ and graphite oxide.

Chapter 6 deals with the improvement in initial discharge behavior by partial decomposition of graphite fluoride in a chlorine atmosphere.

REFERENCES

[1] O. Ruff and O. Bretschneider, Z. Anorg. Allgem. Chem., 217, 1(1934).

[2] W. Rüdorff and G. Rüdorff, Z. Anorg. Allgem. Chem., 253, 281(1947).

[3] W. Rüdorff and G. Rüdorff, Chem. Ber., 80, 413(1947).

[4] W. Rüdorff and G. Rüdorff, ibid., 80, 417(1947).

[5] W. Rüdorff and K. Brodersen, Z. Naturforsch., 12b, 595(1957).

[6] W. Rüdorff, Advan. Inorg. Chem. Radiochem., 1, 230 (1959).

[7] N. Watanabe, Y. Koyama and S. Yoshizawa, Denki Kagaku, 31, 756(1963).

[8] N. Watanabe and K. Kumon, Denki Kagaku, 35, 19(1967).

[9] N. Watanabe and A. Shibuya, Kogyo Kagaku Zasshi, 71,

968(1968).
[10] N. Watanabe and M. Fukuda, U.S. Pat., 3,536,532(Oct. 27, 1970), 3,700,502(1972).
[11] N. Watanabe and M. Takashima, Kogyo Kagaku Zasshi, 74, 1788(1971).
[12] N. Watanabe, Y. Koyama, A. Shibuya and K. Kumon, Mem. Fac. Eng., Kyoto Univ., 33(Pt. 1), 15(1971).
[13] N. Watanabe, H. Takenaka and M. Takashima, Nippon Kagaku Kaishi, 487(1973).
[14] N. Watanabe, M. Takashima and Y. Kita, ibid., 885 (1974).
[15] N. Watanabe, M. Takashima and K. Takahashi, ibid., 1033 (1974).
[16] M. Takashima and N. Watanabe, ibid., 432(1975).
[17] N. Watanabe, H. Takenaka and S. Kimura, ibid., 1655 (1975).
[18] N. Watanabe and Y. Kita, ibid., 1896(1975).
[19] N. Watanabe and Y. Kita, Tanso, 84, 2(1976).
[20] M. Takashima and N. Watanabe, Nippon Kagaku kaishi, 1222(1976).
[21] N. Watanabe, T. Kawaguchi and Y. Kita, ibid., 191 (1977).
[22] N. Watanabe, T. Kawaguchi and Y. Kita, ibid., 1082 (1978)
[23] N. Watanabe and H. Takenaka, Tanso, 92, 2(1978).
[24] N. Watanabe, T. Kawaguchi and Y. Kita, Nippon Kagaku Kaishi, 901(1979).
[25] N. Watanabe and K. Morigaki, Denki Kagaku, 47, 169 (1979).
[26] N. Watanabe and K. Morigaki, ibid., 47, 174(1979).
[27] N. Watanabe, Y. Kita and O. Mochizuki, Carbon, 17, 359(1979).
[28] Y. Kita, N. Watanabe and Y. Fujii, J. Am. Chem. Soc., 101, 3832(1979).
[29] N. Watanabe, Solid State Ionics, 1, 87(1980).

[30] N. Watanabe, M. Endo and K. Ueno, Solid State Ionics, 1, 5016(1980).
[31] N. Watanabe, S. Koyama and H. Imoto, Bull. Chem. Soc. Jpn., 53, 2731(1980).
[32] N. Watanabe and S. Koyama, ibid., 53, 3093(1980).
[33] N. Watanabe, T. Kawamura and S. Koyama, ibid., 53, 3093(1980).
[34] N. Watanabe and K. Ueno, ibid., 53, 388(1980).
[35] N. Watanabe, Physica, 105B, 17(1981).
[36] N. Watanabe, A. Izumi and T. Nakajima, J. Fluorine Chem., 18, 475(1981).
[37] K. Ueno, N. Watanabe and T. Nakajima, J. Fluorine Chem., 19, 323(1982).
[38] N. Watanabe, T. Nakajima and N. Ohsawa, Bull. Chem. Soc., Jpn., 55, 2029(1982).
[39] N. Watanabe, Y. Ashida and T. Nakajima, ibid., 55, 3197(1982).
[40] N. Watanabe, T. Nakajima, M. Kawaguchi and A. Izumi, ibid., 56, 455(1983).
[41] N. Watanabe, S. Katoh, and T. Nakajima, ibid., 57, 701(1984).
[42] H. Touhara, K. Kadono and N. Watanabe and M. Endo, J. Chimie Physique, 81, 841(1984).
[43] H. Touhara, H. Fujimoto, N. Watanabe and A. Tressaud, Solid State Ionics, 14, 163(1984).
[44] N. Watanabe and M. Ishii, Denki Kagaku, 29, 364 (1961).
[45] N. Watanabe, M. Inoue and S. Yoshizawa, Denki Kagaku, 31, 693(1963).
[46] N. Watanabe and M. Nishimura, Yoyuen, 11, 267(1968).
[47] N. Watanabe and T. Asaue, Denki Kagaku, 39, 123 (1971).
[48] H. Imoto, T. Nakajima and N. Watanabe, Bull. Chem. Soc. Jpn., 48, 1633(1975).
[49] H. Imoto and N. Watanabe, Bull. Chem. Soc. Jpn., 49,

1736(1976).
[50] A. K. Kuriakose and J. L. Margrave, J. Phys. Chem., 69, 2772(1965).
[51] A.K. Kuriakose and J. L. Margrave, Inorg. Chem., 4, 1939(1965).
[52] J. L. Wood, R. B. Badachhape, R. J. Lagow and J. L. Margrave, J. Phys. Chem., 73, 3139(1969).
[53] R. J. Lagow, R. B. Badachhape, P. Ficalora, J. L. Wood and J. l. Margrave, Syn. Inorg. Metal-org. Chem., 2, 145(1972).
[54] J. L. Wood, A. J. Valerga, R. B. Badachhape and J. L. Margrave, Final Report, Contact DAABO7-72-C-0105(ECOM), Rice University, Dec. 1972.
[55] A. J. Valerga, R. B. Badachhape, G. D. Parks, P. Kamarchik, J. L. Wood and J. L. Margrave, Final Report, Contact DAABO7-73-C-0056(ECOM), March 1974.
[56] R. J. Lagow, R. B. Badachhape, J. L. Wood and J. L. Margrave, J. Am. Chem. Soc., 96, 2628(1974).
[57] R. J. Lagow, R. B. Badachhape, J. L. Wood and J. L. Margrave, J. Chem. Soc. Dalton, 1268(1974).
[58] V. K. Mahajan, R. B. Badachhape and J. L. Margrave, Inorg. Nucl. Chem. Lett., 10, 1103(1974).
[59] P. Kamarchik Jr. and J. L. Margrave, J. Thermal Anal., 11, 259(1977).
[60] D. E. Palin and K. D. Wadsworth, Nature, 162, 925 (1948).
[61] C. S. Jacobs and K. D. Wadsworth, Brit. Pat. 759173 /1956(to ICI).
[62] R. J. Lagow, L. A. Shimp, D. K. Lam and R. F. Baddour, Inorg. Chem., 11, 2568(1972).
[63] M.L. Bernard, A. Hardy, P. Hobbes, R. Lucas and M. Roux, Bull. Soc. Chem. Fr., 2129(1972).
[64] D. E. Parry, J. M. Thomas, B. Bach and E. L. Evans, Chem. Phys. Lett., 29, 128(1974).
[65] L. B. Ebert, J. I. Brauman and R. A. Huggins, J. Am.

Chem. Soc., 96, 7841(1974).
[66] D. T. Clark and J. Peeling, J. Polym. Sci. Chem. Ed., 14, 2941(1976).
[67] P. Cadman, J. D. Scott and J. M. Thoman, Carbon, 15, 75(1977).
[68] C. A. Wilke, G. Yu Lin and D. T. Howarth, J. Solid State Chem., 30, 197(1979).
[69] Y. Ishihara and T. Shimada, 5th International Fluorine Symposium, Moscow, 1969.
[70] R. L. Fusaro and H. E. Sliney, A.S.L.E. Trans., 13, 56(1970).
[71] H. Gisser, M. Petronio and A. Shapiro, International Conf. of Solid Lubrication, Denver, August, 1971.
[72] H. Gisser, M. Petronio and A. Shapiro, Lubric. Eng., 28, 161(1972).
[73] R. L. Fusaro and H. E. Sliney, A.S.L.E. Trans., 16, 189(1973).
[74] Y. Tsuya, H. Uemura, Y. Okamoto and S. Kurosaki, ASLE/ ASME Lubric. Conf., Atlanta, 1973.
[75] Ch. Martin, J. Sullean and M. Roussel, Wear, 34, 215 (1975).
[76] M. Fukuda and T. Iijima, in Power Sources 5, ed. D. H. Collins, Academic Press: London & New York, 713(1975).
[77] R. G. Gunther, ibid., 729(1975); idem, U. S. Pat. 3,892,590/1975(to Yardney Int. Corp.).
[78] M. Fukuda and T. Iijima, Progress in Batteries and Solar cells, 1, 26(1978).
[79] J. Watanabe, H. Ogawa and R. Okazaki, ibid., 1, 39 (1978).
[80] J. Watanabe, E. Kawakubo, T. Shinagawa and Y. Kajikawa, ibid., 3, 74(1980).
[81] N. Watanabe and T. Nakajima, Preparation Properties and Industrial Applications of Organofluorine Compounds, Ellis Horwood, Ch. 9(1982).
[82] A. Kozawa, U. S. Pat. 3,956,018(1976).

[83] H. F. Hunger and G. J. Heymach, J. Electrochem. Soc., 120, 1161(1973).
[84] H. F. Hunger and J. E. Ellison, ibid., 122, 1288 (1975).
[85] W. Tiedemann, ibid., 121, 1308(1974).
[86] M. S. Whittingham, ibid., 122, 526(1975).
[87] K. Ueno, N. Watanabe and T. Nakajima, J. Fluorine Chem., 19,323(1982).

Chapter 1

ELECTRODE REACTION OF GRAPHITE FLUORIDE AS CATHODE ACTIVE MASS

1. INTRODUCTION

It was about fifteen years ago that the lithium-graphite fluoride cell in nonaqueous electrolyte system was proposed as a primary battery. Since then several mechanisms have been proposed on the reaction of graphite fluoride cathode. Margrave et al. calculated the theoretical electromotive force(EMF) of 4.57 V for Li-$(CF)_n$ cell from calorimetry on the assumption that the total cell reaction was as follows (1);

$$CF + Li \longrightarrow C + LiF. \qquad [1-1]$$

However, the EMF of a real cell is around 3.2-3.3 V when 1M-$LiClO_4$-propylene carbonate is used as an electrolyte. To explain this EMF difference, Whittingham(2) proposed the cell reaction in which the discharge product is not the graphite and LiF but the ternary graphite intercalation compound composed of C, Li and F;

$$CF + xLi \longrightarrow CLi_xF. \qquad [1-2]$$

Watanabe et al.(3-5) made a series of analyse on the discharge product and confirmed the existence of ternary compound including the propylene carbonate along with the graphite-like carbon and LiF. However, the amount of ternary compound is so thin that the structural analysis by means

---

Electrochim. Acta, 27, 1615(1982).
To be submitted to J. Electrochem. Soc..

of X-ray diffractometry has not yet been succeeded.

In this chapter electrode reactions of two types of graphite fluorides, $(CF)_n$ and $(C_2F)_n$ were studied on the basis of electrochemical measurements. The effects of the electrolyte solvents on the electrode reaction were investigated using several kinds of organic solvents. A cathode model and formulation of electrode potential are also presented.

2. EXPERIMENTAL

2-1 Preparation of graphite fluorides

$(CF)_n$ and $(C_2F)_n$-type graphite fluorides were prepared by direct fluorination of Madagascar natural graphite(51-61 μm, purity 99.4%) in a nickel reaction tube. The structural analysis was performed by X-ray diffraction powder method. The elemental analyse of carbon and fluorine were made at the Laboratory for Organic Elemental Micro-analysis of Kyoto University. The synthetic conditions and the analytical data are listed in Table 1-1.

Table 1-1 Synthetic conditions and analytical data of graphite fluorides

	$(CF)_n$	$(C_2F)_n$
Synthetic conditions		
Pristine carbon	Madagascar natural graphite	
Fluorine pressure/mmHg	760	700
Reaction temperature/°C	590	390
Reaction time/h	24	168
Analytical data		
F/C ratio	1.00	0.61
d(002)/nm	0.59	0.81
β(002)/°	1.4	2.9

2-2 Preparation of graphite fluoride cathodes

These graphite fluorides weighing 10mg were well mixed with 10 mg of acetylene black as a conductive additive and 10 mg of polyethylene as a binder. The mixture was sandwiched between filter papers and molded into a pellet of 9.0 mm in diameter and 1 mm in thickness under a pressure of 400-700 MPa. Carbon fiber as a terminal was wound around the edge of the pellet. It was then covered with a polyethylene tube, the tip of which was welded with the edge of a pellet to fix the electrode.

2-3 Anode and reference electrode

A piece of lithium metal(purity 99%) was quarried out from a block, and was pressed on a nickel screen connected to a terminal nickel wire covered with a polyethylene tube. Reference electrode was also lithium metal pressed on the ribbon of nickel screen.

2-4 Solvents and electrolytes

Four kinds of solvents: dimethyl sulfoxide(DMSO), γ-butyrolactone(BL), propylene carbonate(PC) and sulfolane (TMS)(purity 98-99%) were used as solvents of nonaqueous electrolyte solutions. These solvents were vacuum-distilled and stored in a sealed flask with 5A molecular sieves. Lithium perchlorate, $LiClO_4$(purity 99.9%) as an electrolyte was dried under vacuum at 200°C for several days, then dissolved in the purified solvents so as to be 1M solutions. Water content was confirmed to be less than 100 ppm by Karl Fischer titration.

2-5 Cell construction and electrochemical measurements

A glass cell used was so constructed that two lithium anodes might face both sides of graphite fluoride cathode and a cathode potential was monitored by lithium reference electrode through a ruggin capillary(Fig. 1-1). Voltage was

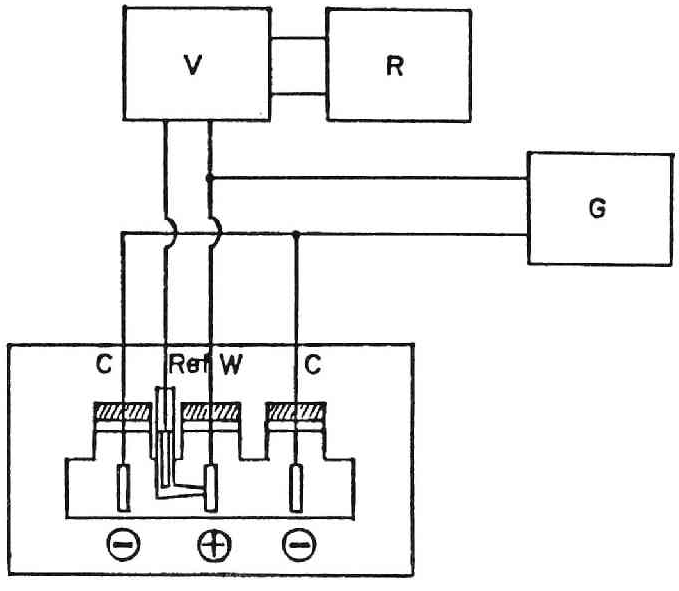

Fig. 1-1 Experimental apparatus

measured with an operation amplifier having an internal impedance of 10^{12} Ω, and was corrected by a small IR drop between cathode and the tip of the ruggin capillary measured with the current interrupter method. All the measurements were carried out in a glove box of argon atmosphere. Temperature was kept constant at 25°C. After cell construction, the open circuit voltage(OCV) was stabilized for one day prior to discharge. The cells were discharged at a fixed current density(geometrical surface area of the electrode was $1.27cm^{-2}$.), using a potentiostat/galvanostat(Hokuto Denko Co. Ltd., HA-301).

3. RESULTS AND DISCUSSION

3-1 Discharge characteristics of graphite fluorides

Figure 1-2 shows discharge curves of $(CF)_n$ and $(C_2F)_n$ electrodes at the apparent current densities of

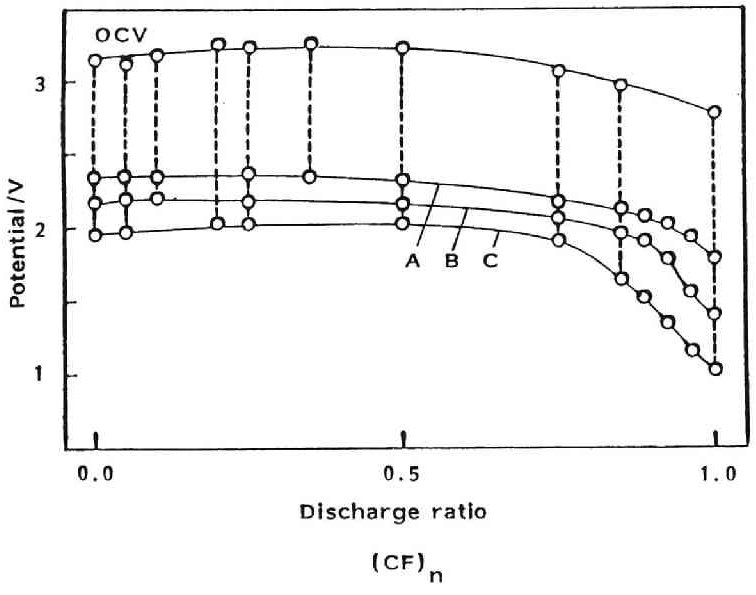

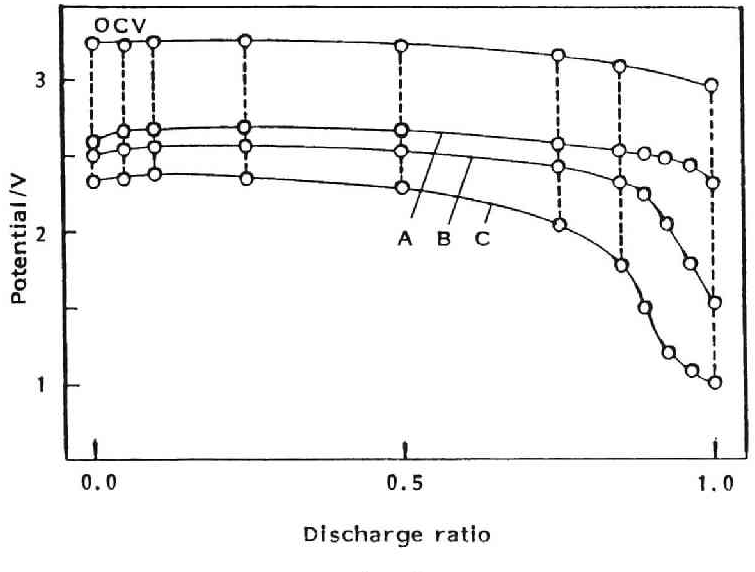

Fig. 1-2 Discharge curves of graphite fluoride electrodes
(1M $LiClO_4$-PC solution, 25°C)
A: 0.01 $mAcm^{-2}$, B: 0.1 $mAcm^{-2}$, C: 0.5 $mAcm^{-2}$.

0.01, 0.1 and 0.5 $mAcm^{-2}$ when the 1M $LiClO_4$-PC solution was used as an electrolyte. A flat discharge potential was observed at every current density until the discharge ratio reached around 70-80% for both $(CF)_n$ and $(C_2F)_n$. Open circuit voltages also gave a constant value of 3.2-3.3 V, hence the overpotential being maintained to be constant in this range. Constant OCV and CCV independent of the discharge ratio suggest that the reaction proceeds heterogeneously. Namely, activity or concentration of species determining the electrode potential are maintained constant by phase separation of the discharge product, differently from the electrodes such as TiS_2, discharge of which proceeds homogeneously making the Li_xTiS_2 where lithium concentration, hence the electrode potential, changes with the discharge ratio, x(6).

The thermodynamic and structural studies mentioned above suggest the existence of ternary phase composed of carbon, fluorine and lithium. However the quantity of this phase in the discharge product is so small that it can be detected only by the aid of ESCA and NMR measurements both of which showed bondings among carbon, fluorine and lithium are semi-ionic.(3-5). X-ray diffraction measurement detected only the graphite-like carbon and LiF. From the results above, it is expected that the discharge reaction is the formation of the ternary phase followed by its decomposition.

3-2 The cathode potentials in different solvents

Lithium metal as a reference electrode indicates different potentials in each solvent due to the difference in lithium ion solvation energy. It is necessary to correct the difference in the potentials of reference electrode to compare the potentials of graphite fluoride electrodes in different solvents. The free energy of solvation for a single ion can be estimated from appropriate models(7).

Here modified Born's equation(8-11) was employed. In this method, an ion is regarded as a rigid sphere of radius r bearing a charge ze, then the free energy of solvation is obtained by calculating the change in the Gibbs' free energy on transferring of this charged sphere from vacuum into a solvent whose dielectric constant is ε, as follows;

$$\Delta G_{solv} = -\frac{Ne^2}{2}\left(1 - \frac{1}{\varepsilon}\right)\left(\frac{Z^2}{r + r'}\right) \qquad [1-3]$$

where N is Avogadro's number and r' is the correction factor to take into account the dielectric saturation, formation of covalent bonds and so on(10). The solvation energies calculated by eq. 1-3 are -5.00×10^5, -4.80×10^5, -4.56×10^5 and -4.58×10^5 $Jmol^{-1}$-Li^+ for DMSO, BL, PC and TMS, respectively. The differences of these solvation free energies correspond to the differences in lithium electrode potentials in the solvents and the potentials of lithium electrodes relative to that in 1M $LiClO_4$-PC solution are -0.45 V in DMSO, -0.25 V in BL at 25°C and -0.02 V in TMS at 30°C.

The OCV's of lithium-$(CF)_n$ and $(C_2F)_n$ batteries and the single electrode potentials in the four kinds of solvents are listed in Table 1-2, where the OCV's at the time of cell construction, before discharge and after 25% discharge were not the same as each other. This may be due to the influence of the terminal groups such as $>CF_2$ and $-CF_3$ on the surface of graphite fluoride and adsorbed oxygen on acetylene black. The OCV's after 25% discharge show high reproducibilities, being regarded as the equilibrium potential of lithium-graphite fluoride batteries. Though the cell using TMS was operated at the temperature by 5°C higher than others, the diference in the OCV's was less than 0.01V. Table 1-2 shows that the OCV's of lithium-$(CF)_n$ and $(C_2F)_n$ batteries are almost equal to each other, which means that the free energy changes of the cell

Table 1-2 OCV's of lithium-graphite fluoride cells and single electrode potentials of cathodes in different solvents(V)

Solvents (1M $LiClO_4$ solution)	At cell construction		Just before discharge		At 25% discharge	
	CF	C_2F	CF	C_2F	CF	C_2F
DMSO	3.49	3.50	3.34	3.33	3.50	3.47
	(3.04)	(3.05)	(2.89)	(2.88)	(3.05)	(3.02)
BL	3.25	3.21	3.26	3.24	3.30	3.39
	(3.00)	(2.95)	(3.01)	(2.99)	(3.05)	(3.14)
PC	3.14	3.17	3.22	3.31	3.28	3.26
	(3.14)	(3.17)	(3.22)	(3.31)	(3.28)	(3.26)
TMS	3.13	3.25	3.17	3.27	3.28	3.27
	(3.11)	(3.23)	(3.15)	(3.25)	(3.26)	(3.25)

The values in parentheses indicate single electrode potentials relative to $Li/Li^+(1M)(PC)$.

reaction are almost the same. The recovery to OCV after cut-off of the circuit takes a very long time for both $(CF)_n$ and $(C_2F)_n$ as will be discussed in Chapter 2. Both lithium-$(CF)_n$ and $(C_2F)_n$ cells indicated different OCV's in different solvents, which suggests the participation of the solvent in the cell reactions.

Figure 1-3 is the plot of single electrode potentials of graphite fluoride in four kinds of solvents as a function of free energy changes of lithium ion solvation. In both cases of $(CF)_n$ and $(C_2F)_n$, the electrode potential of graphite fluoride decreases with increasing solvation free energy for lithium ion. However, as can be seen from Fig. 1-3, electrode potential decreases by about a half of solvation energy, namely the slope of the straight line is close to about 0.5. If the desolvation are completed and

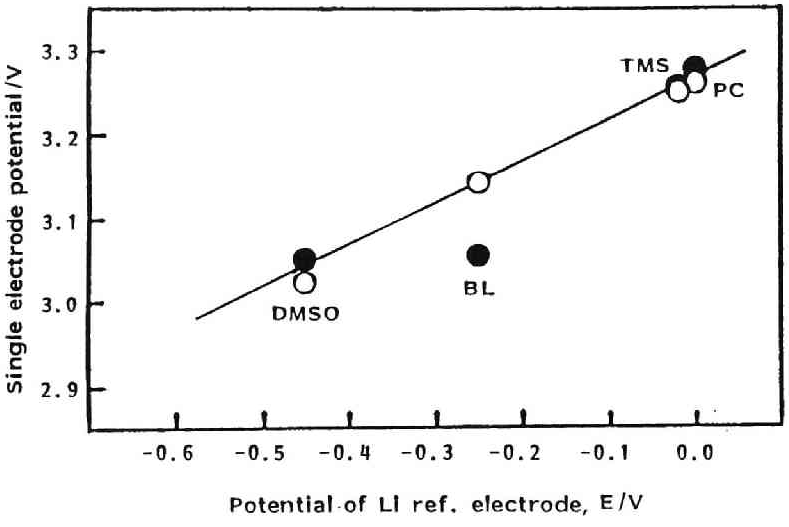

Fig. 1-3 Single electrode potential of graphite fluoride electrode vs solvation free energy for lithium ion

$E=\Delta\Delta G_{solv}/nF(V)$. $\Delta\Delta G_{solv}=\Delta G_{solv}(solvent) - \Delta G_{solv}(PC)$.

● : $(CF)_n$ ○ : $(C_2F)_n$

the solvent doesn't participate in the cell reaction as expressed by eq. 1-1, the slope might be unity, in other words, OCV's must be the same among these solvents. The graphite fluoride electrode shows the lower potential in the solvent where lithium ion is more strongly solvated. If the lithium ion is intercalated into the graphite fluoride layers together with the solvent molecules making a solvated ternary graphite intercalation compound, the more strongly the lithium ion is solvated, the lower is the ability for solvated lithium ion to make an ion pair with fluoride ion. As a result, the activity of fluoride ion becomes higher and the electrode potential would be lowered. The solvation numbers are around 4 for the solvents used here(12), however, it may become less than that if the partial desol-

vation occurs through the process of making an ion pair between lithium and fluoride ions. Such reaction in which a solvated ion is intercalated is observed not only in other graphite intercalation compounds(13) but also in some transition metal dicalcogenides(6).

The influence of solvent molecule on the electrode kinetics will be discussed in Chapter 3, which is also one of the proof that the solvent molecule participates in the electrode reaction.

3-3 Thermodynamics of electrode reaction

From the above results, it is concluded that the total cell reaction of lithium-graphite fluoride cell is the formation of ternary solvated graphite intercalation compound(GIC);

$$C_xF + Li + zS \longrightarrow C_xF^- \cdot Li^+ \cdot zS. \qquad [1-4]$$

where x=1 for $(CF)_n$ and 2 for $(C_2F)_n$. S and z are solvent molecule of electrolyte solution and solvation number for lithium ion in the discharge product. Discharge product in [1-4] is decomposed by the following disproportionation reaction;

$$C_xF^- \cdot Li^+ \cdot zS \longrightarrow xC + LiF + zS. \qquad [1-5]$$

In this way, a kind of GIC phase exists as a thin film connected with the edge of graphite fluoride crystallite. Disproportionation reaction proceeds chemically, namely the charge transfer between two different phases doesn't occur. The EMF of a real cell is around 3.2-3.3 V which is considered to correspond to the free energy change for the cell reaction [1-4]. Therefore the difference between EMF's of reaction [1-1] and [1-4] is attributed to the free energy change in reaction [1-5] which cannot be converted to the

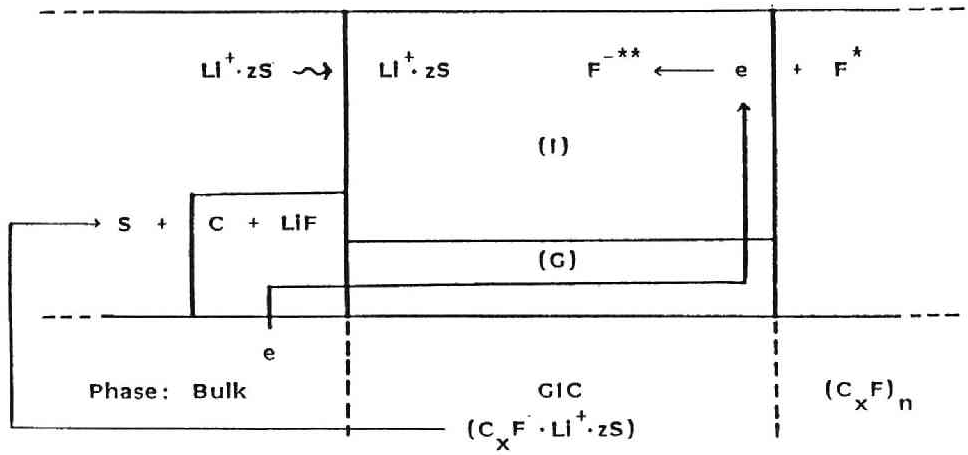

Fig. 1-4 Schematic illustration of graphite fluoride electrode

(I) Intercalate(Guest) layer

(G) Graphene(Host) layer

F*: covalently bonded to sp^3 carbon

F**: semi-ionically bonded to sp^2 carbon

electrical energy, but consumed as the heat in the cell.

At equilibrium state, separate equilibria involving electrons, fluoride and lithium ions between adjacent two phases must be taken into account(Fig. 1-4).

$$\bar{\mu}_{e}^{GIC(G)} = \bar{\mu}_{e}^{CxF} \qquad [1-6]$$

$$\bar{\mu}_{F^-}^{CxF} = \bar{\mu}_{F^-}^{GIC(I)} \qquad [1-7]$$

$$\bar{\mu}_{Li^+}^{GIC(I)} = \bar{\mu}_{Li^+}^{B} \qquad [1-8]$$

where $\bar{\mu}_i^{\alpha}$ is the electrochemical potential of species i in phase α. Symbols (G) and (I) mean electrically conductive graphene layer and ionically conductive intercalate layer, respectively. From eq. 1-6,

$$\mu_e^{GIC(G)} - F\Phi^{GIC(G)} = \mu_e^{CxF} - F\Phi^{CxF} \qquad [1\text{-}9]$$

where μ_i^{α} is the chemical potential of species i in phase α and Φ^{α} is inner potential(Galvani potential) in phase α. Hence

$$\Phi^{GIC(G)} - \Phi^{CxF} = \frac{\mu_e^{GIC(G)} - \mu_e^{CxF}}{F} = \frac{\mu^{\circ}{}_e^{GIC(G)} - \mu^{\circ}{}_e^{CxF}}{F} \qquad [1\text{-}10]$$

Symbol "°" means a standard state. Similarly from eq. 1-7,

$$\mu_{F^-}^{CxF} - F\Phi^{CxF} = \mu_{F^-}^{GIC(I)} - F\Phi^{GIC(I)} \qquad [1\text{-}11]$$

For chemical potentials of fluoride ion in C_xF and GIC(I) phases, the following equations are derived.

$$\mu_{F^-}^{CxF} = \mu^{\circ}{}_{F^-}^{CxF} \qquad [1\text{-}12]$$

$$\mu_{F^-}^{GIC(I)} = \mu^{\circ}{}_{F^-}^{GIC(I)} + RT\ln a_{F^-}^{GIC(I)} \qquad [1\text{-}13]$$

Symbol a_i^{α} is the activity of species i in phase α. From eq. 1-11,12 and 13,

$$\Phi^{CxF} - \Phi^{GIC(I)} = \frac{\mu^{\circ}{}_{F^-}^{CxF} - \mu^{\circ}{}_{F^-}^{GIC(I)}}{F} - \frac{RT}{F}\ln a_{F^-}^{GIC(I)} \qquad [1\text{-}14]$$

Similarly from eq. 1-8,

$$\mu_{Li^+}^{GIC(I)} + F\Phi^{GIC(I)} = \mu_{Li^+}^{B} + F\Phi^{B} \qquad [1\text{-}15]$$

$$\mu_{Li^+}^{GIC(I)} = \mu^{\circ}{}_{Li^+}^{GIC(I)} + RT\ln a_{Li^+}^{GIC(I)} \qquad [1\text{-}16]$$

$$\mu_{Li^+}^{B} = \mu^{\circ}{}_{Li^+}^{B} + RT\ln a_{Li^+}^{B} \qquad [1\text{-}17]$$

From eq. 1-15, 16 and 17,

$$\phi^{GIC(I)} - \phi^{B} = \frac{\mu^{\circ B}_{Li^+} - \mu^{\circ GIC(I)}_{Li^+}}{F} + \frac{RT}{F}\ln \frac{a^{B}_{Li^+}}{a^{GIC(I)}_{Li^+}} \qquad [1\text{-}18]$$

By adding eq. 1-10, 14 and 18,

$$\phi^{GIC(G)} - \phi^{B} = \frac{\mu^{\circ GIC(G)}_{e} - \mu^{\circ CxF}_{e} + \mu^{\circ CxF}_{F^-} - \mu^{\circ GIC(G)}_{F^-} + \mu^{\circ B}_{Li^+} - \mu^{\circ GIC(I)}_{Li^+}}{F}$$

$$- \frac{RT}{F}\ln \frac{a^{GIC(I)}_{Li^+} \cdot a^{GIC(I)}_{F^-}}{a^{B}_{Li^+}} \qquad [1\text{-}19]$$

The potential of lithium reference electrode can be written as follows;

$$\phi^{Li} - \phi^{B} = \frac{\mu^{\circ B}_{Li^+} - \mu^{\circ Li}_{Li^+}}{F} + \frac{RT}{F}\ln a^{B}_{Li^+} \qquad [1\text{-}20]$$

From eq. 1-19 and 20,

$$E = \phi^{GIC(G)} - \phi^{Li} = E_1^{\circ} - \frac{RT}{F}\ln\left(a^{GIC(I)}_{Li^+} \cdot a^{GIC(I)}_{F^-} \right) \qquad [1\text{-}21]$$

where

$$E_1^{\circ} = \frac{\mu^{\circ GIC(G)}_{e} - \mu^{\circ CxF}_{e} + \mu^{\circ CxF}_{F^-} - \mu^{\circ GIC(I)}_{F^-} - \mu^{\circ GIC(I)}_{Li^+} + \mu^{\circ Li}_{Li^+}}{F}$$

Eq. 1-21 indicates that the cathode potential relative to lithium reference electrode varies with the product of activities of lithium and fluoride ions in GIC(I) phase.

3-4 Electron conduction mechanism in graphite fluoride electrode

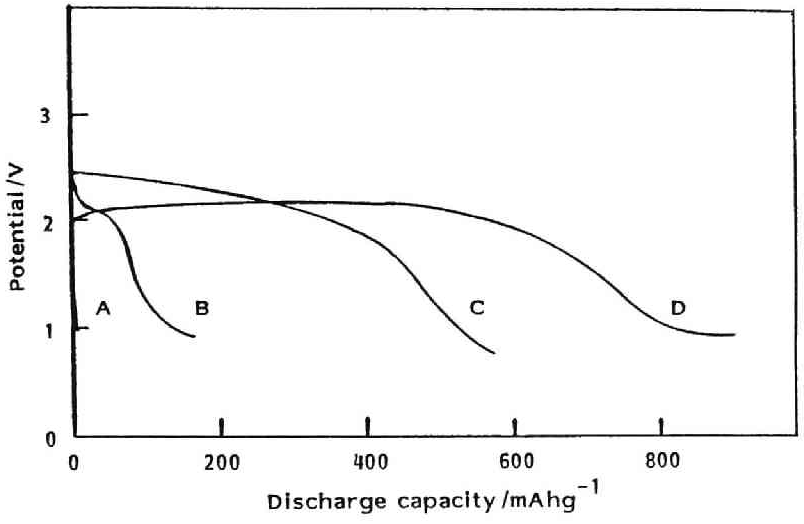

Fig. 1-5 Discharge characteristics of several fluorocarbons (1M $LiClO_4$-PC solution, 0.5 $mAcm^{-2}$, 25°C)

A: Polytetrafluoroethylene
B: $C_{24}F_{36}$(Perfluorocoronene)
C: $(CF)_n$ prepared from non-heat-treated petroleum coke
D: $(CF)_n$ prepared from Madagascar natural graphite

During the discharge, solvated lithium ions are intercalated in graphite fluoride, making a thin layer of a ternary graphite intercalation compound which decomposes by the subsequent disproportionation reaction. This maintains the thickness of the diffusion layer constant to give a flat discharge potential as shown in Fig. 1-2. An electron can be transferred to the surface of graphite fluoride through a GIC(G) and carbon phase produced by decomposition of GIC (Fig 1-4).

Figure 1-5 shows the discharge curves of several kinds of fluorocarbons. Physical and chemical properties are listed in Table 1-3. Perfluorocoronene is prepared as a by-product of $(CF)_n$ from non-heat-treated petroleum coke, the

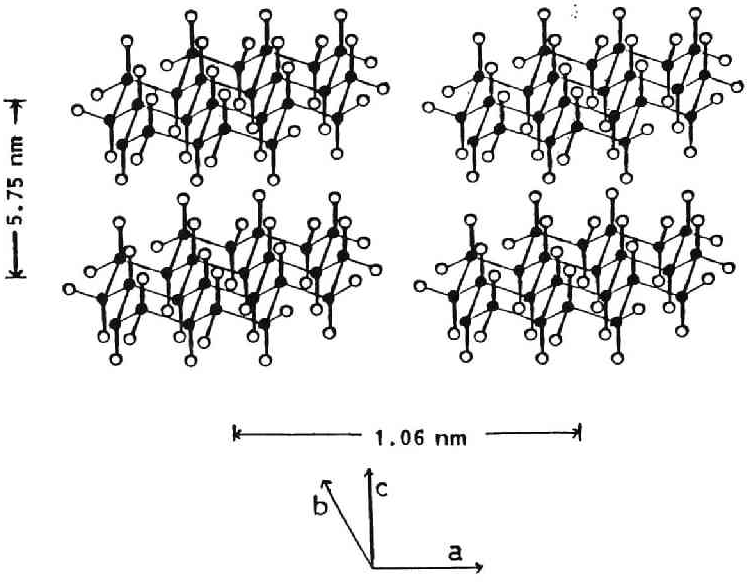

Fig. 1-6 Crystal structure of $C_{24}F_{36}$

● : C ○ : F

Table 1-3 Physical and chemical properties of fluorocarbons

Fluorocarbons	Empirical formula	F/C	Carbon framework	Specific reistance/ Ωcm
Polytetrafluoroethylene	CF_2	2	straight chain	$>10^{14}$
Perfluorocoronene	C_2F_3	1.5		--
$(CF)_n$ prepared from non-heat-treated petroleum coke	CF	1	trans-linked cyclohexane chairs	$>10^{20}$
$(CF)_n$ prepared from Madagascar natural graphite	CF	1		$>10^{20}$

structure of which is shown in Fig. 1-6. This compound can be purified by sublimation at around 150°C(14).

The chemical bonds between carbon and fluorine of these fluorocarbons are essentially the same, covalent. As shown in Table 1-3, these compounds are electrical insulators. However the difference in the "electrochemical activity" between polytetrafluoroethylene and others are obvious in Fig. 1-5. It is due to the difference in carbon framework among these fluorocarbons. The former is composed of the straight chain and the latters are composed of trans-linked cyclohexane chairs stacked along C axis. The most thermodynamically stable phase of carbon at ambient temperature and pressure is graphite, however, graphitization needs a high activation energy for cyclization, aromatization and crystal growth. On the other hand, the carbon framework of graphite fluoride can easily revert graphite structure in the cathode reduction process as can be seen by X-ray diffractometry of the discharge product.

With decreasing the size of arrays of cyclohexane chairs along ab axis in graphite fluoride, the discharge capacity and utility of fluorine decreased. It would be due to the destruction of graphite fluoride structure by expansion along C axis with the intercalation of large solvated lithium ions which prevents the recovery of graphite structure by discharge, namely localization of electrons occurs in benzene rings recovered by discharge. The ratio of undischarged fluorine in graphite fluoride would increase as the decrease of its initial crystallite size.

As it turns out, the ternary phase is the electron path to the surface of graphite fluoride through the GIC(G) phase, besides the lithium ion path through GIC(I) phase, which makes the discharge of an electrical insulator possible.

4. SUMMARY

(1) OCV's of lithium-$(CF)_n$ and $(C_2F)_n$ were nearly the same. OCV's increased with increasing the solvation energy of the solvent used, which indicates the cointercalation of the solvent molecules in the graphite fluoride. The discharge reaction of lithium-graphite fluoride is therefore the formation of a thin layer composed of ternary graphite intercalation compound (GIC) with solvent molecule, followed by the decomposition to carbon, LiF and solvent.
(2) Cathode potential relative to lithium reference electrode varies with the product of activities of lithium and fluoride ions in GIC(I) phase.
(3) With decreasing size of arrays of cyclohexane rings along ab axis in graphite fluoride, the capacity and utility of fluorine decreased. This would be due to the difficulty in recovery of electroconductive graphite structure by discharge.

REFERENCES

[1] A. J. Valerga, R. B. Badachhape, G. D. Parks, P. Kammarchick, J. L. Wood, and J. L. Margrave, Final Report, Contact DAAB 07-73-c-0056(ECOM), Rice University, Austin, TX(1974).
[2] M. S. Whittingham, J. Electrochem. Soc., 122, 526 (1975).
[3] N. Watanabe and K. Morigaki, Denki Kagaku, 47, 174 (1979).
[4] N. Watanabe, Solid State Ionics, 1, 87(1980).
[5] H. Touhara, H. Fujimoto, N. Watanabe and A. Tressaud, ibid., 14, 163(1984).
[6] M. S. Whittingham., Prog. Solid St. Chem., 12, 41 (1978).
[7] J. Burgess, Metal Ions in Solutions, Ch. 7. Ellis

Horwood Limit, New York(1978).
[8] M. Born, Z. Physik, 1, 45(1920).
[9] W. M. Latimer, K. S. Pitzer and C. M. Slanski, J. Chem. Phys., 7, 108(1939).
[10] N. Matsuura, K. Umemoto, M. Waki, Z. Takeuchi and M. Omoto, Bull. Chem. Soc. Japan, 47, 810(1974).
[11] N. Tanaka and T. Ogata, Inorg. Nucl. Chem. Lett., 10, 511(1974).
[12] R. A. Horne, Water and Aqueous Solutions, Ch. 4, Wiley-Interscience, New York(1972).
[13] F. Beguin and R. Setton, Carbon, 13, 293(1975).
[14] N. Watanabe, S. Katoh and T. Nakajima, Bull. Chem. Soc. Jpn., 57, 701(1984).

Chapter 2

ELECTRODE KINETICS OF GRAPHITE FLUORIDE IN THE LITHIUM CELL

1. INTRODUCTION

It has been suggested that the cathode overpotential of lithium-graphite fluoride cell has been pointed out to be due to the delay of lithium ion transfer in graphite fluoride. The current density of a commercial battery is limited less than several tens of microampere per square centimeters because of a large overpotential of the cathode.

In this chapter, some kinetic parameters were obtained by transient techniques, and the electrode kinetics of graphite fluorides are discussed.

2. THEORETICAL CONSIDERATIONS

2-1 Introduction of thermodynamic factor

Formulation of the potential of graphite fluoride cathode was made in Chapter 1, where eq. 1-21 indicates that the cathode potential relative to lithium reference electrode varies with the product of activities of lithium and fluoride ions in GIC(I) phase. In the present case, eq. 1-21 is applicable not only to the equilibrium state but also to the non-equilibrium state because the charge transfer is considered to be much faster than the diffusion rate of a solvated lithium ion in GIC(I) phase.

Eq. 1-21 can be rewritten as follows;

To be submitted to J. Electrochem. Soc..

$$E = E_1^\circ - \frac{\ln\left(a_{Li^+}^{GIC(I)} \cdot a_{F^-}^{GIC(I)}\right)}{\ln C_{Li^+}^{GIC(I)}} \cdot \frac{RT}{F} \ln C_{Li^+}^{GIC(I)} \qquad [2\text{-}1]$$

where C is the concentration of Li^+ ion. In GIC phase, lithium ion is mobile while fluorine atom cannot change its position. The charge of fluoride ion is given by electron via graphene layer because the chemical interaction remains between graphene and fluorine as shown in eq. 1-4. When only one ionic species is transported and the host material has a high electrical conductivity, the ratio of logarithm of activity product to that of concentration can be regarded as Wagner's enhancement factor(1) when it is a constant value;

$$W = \frac{\partial \ln a_{Li}^{GIC(I)}}{\partial \ln C_{Li^+}^{GIC(I)}} = \frac{\partial \ln a_{Li^+}^{GIC(I)} + \partial \ln a_{e}^{GIC(I)}}{\partial \ln C_{Li^+}^{GIC(I)}}$$

$$= \frac{\partial \ln a_{Li^+}^{GIC(I)} + \partial \ln a_{F^-}^{GIC(I)}}{\partial \ln C_{Li^+}^{GIC(I)}} = \frac{\partial \ln\left(a_{Li^+}^{GIC(I)} \cdot a_{F^-}^{GIC(I)}\right)}{\partial \ln C_{Li^+}^{GIC(I)}}$$

$$= \frac{\ln\left(a_{Li^+}^{GIC(I)} \cdot a_{F^-}^{GIC(I)}\right)}{\ln C_{Li^+}^{GIC(I)}} = \text{const.} \qquad [2\text{-}2]$$

The chemical diffusion coefficient, D can be related with the component diffusion coefficient, D^*, which is estimated with several methods such as tracer diffusion

experiment and relaxation time measurement in NMR study.

$$D = D^{*}W \qquad [2-3]$$

The value W is generally calculated from the discharge ratio dependence of OCV. In the case of lithium ion diffusion in Li_xTiS_2, W was in the range from 2 to 60(2). However, for the graphite fluoride electrode, W cannot be calculated by measuring OCV because the discharge reaction proceeds heterogeneously accompanied with little change of OCV. So the estimation was carried out by measuring decay of polarization of the electrode, which will be discussed below.

2-2 Analysis of decay of polarization

Figure 2-1 shows the schematic illustration of off time behavior of the potential of graphite fluoride electrode. Polarization decays very slowly to OCV for one hundred hours or more when the recovery starts from CCV at 0.5 $mAcm^{-2}$.

In Figure 1-4, potential gradient in GIC phase can be neglected compared to concentration gradient because of high electrical conductivity in GIC phase, and a linear and semi-

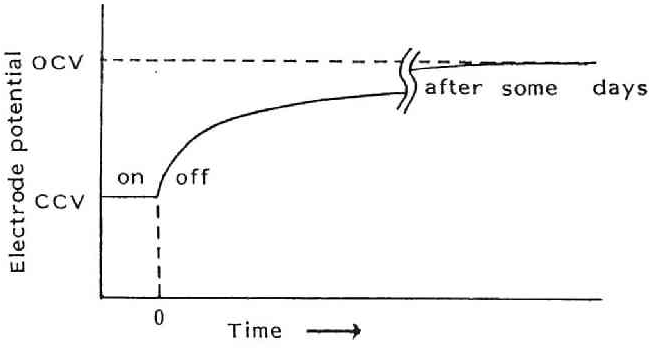

Fig. 2-1 Potential recovery curve of graphite fluoride electrode

infinite diffusion is applied for relatively short period compared to recovery time to OCV. At t=0 the amount of lithium ion inside GIC(I) phase (x>0) can be neglected compared to that at the surface(x=0), and the decrease in concentration of lithium ion by the disproportionation reaction at the surface of GIC phase is relatively smaller than that by diffusion after the circuit is opened, the solution for the equation of Fick's 2nd law,

$$\frac{\partial C(x,t)}{\partial t} = D\frac{\partial C^2(x,t)}{\partial x^2} \qquad [2\text{-}4]$$

is as follows,

$$C(x,t) = \frac{C(0,0)\delta}{2\sqrt{\pi Dt}} \exp\left(\frac{-x^2}{4Dt}\right) \qquad [2\text{-}5]$$

where C(0,0) is the concentration of lithium ions at x=0 and t=0, and $C(0,0)\delta$ is surface concentration. Here D is assumed to be constant and independent of the concentration change. At the electrode surface,

$$C(0,t) = \frac{C(0,0)\delta}{2\sqrt{\pi Dt}} \qquad [2\text{-}6]$$

From eq. 2-1, 2 and 6,

$$E = E_2 + \frac{WRT}{F}\ln\sqrt{t} \qquad [2\text{-}7]$$

where

$$E_2 = E_1^\circ - \frac{WRT}{F}\ln\frac{C(0,0)\delta}{2\sqrt{\pi D}}$$

From the slope of E-ln $\sqrt{t}$ plots, the thermodynamic factor W is obtained.

2-3 Chronoamperometry by single potential step method

When the potential step is imposed on the graphite

fluoride electrode, lithium ions are transported in GIC(I) phase by the concentration gradient. During the potential step, lithium ion concentration is maintained to be a constant value of C_s at the surface of GIC(I) phase(x=0, see Fig. 1-4). At t=0, just before the potential is stepped, lithium ion concentration in GIC(I) phase(x>0) can be neglected compared to the surface concentration of C_s(x=0). Additionally concentration gradient is always zero at x=L. Time-dependent current i(t) is related with Fick's first law

$$i(t) = -FAD\left(\frac{\partial C(x,t)}{\partial x}\right)_{x=0} \qquad [2\text{-}8]$$

where A is the surface area. Current-time relation is derived for the small value of t(Cottrell equation)

$$i(t) = FAD^{1/2}C_s/\pi^{1/2}t^{1/2} \qquad t<<L^2/D \qquad [2\text{-}9]$$

Total amount of charge transfer during the potential step, Q, is related to C_s

$$Q = FALC_s \qquad [2\text{-}10]$$

From eq. 2-9 and 10,

$$i(t) = \frac{QD^{1/2}}{L\pi^{1/2}} \cdot \frac{1}{\sqrt{t}} \qquad [2\text{-}11]$$

The slope of $i - 1/\sqrt{t}$ plots and Q determined by coulometric analysis give the kinetic parameter including diffusion coeficient.

3. EXPERIMENTAL

Synthetic conditions and analytical data of both $(CF)_n$ and $(C_2F)_n$ used in this experiment was the same

as shown in Chapter 1. Preparation of graphite fluoride cathode, lithium metal anode, reference electrode and cell construction were also performed in the same manner. 1M $LiClO_4$-propylene carbonate solution (water content was less than 100 ppm) was used as electrolyte.

Polarization decay curve was obtained at 25°C and potential step experiment was made at 0, 25 and 43°C. The cell temperature was monitored by means of calibrated copper-constantan thermocouple. All the experiments were performed in a dry box of argon atmosphere.

4. RESULTS AND DISCUSSION

4-1 Chronopotentiometry

Figure 1-2 in Chapter 1 shows discharge curves of $(CF)_n$ and $(C_2F)_n$ electrodes at the apparent current densities of 0.01, 0.1 and 0.5 $mAcm^{-2}$ at 25°C. A flat discharge potential was observed at every current density until the discharge ratio reached around 70-80% for both $(CF)_n$ and $(C_2F)_n$. Open circuit voltages also gave a constant value of 3.2-3.3 V, hence the overpotential being maintained to be constant in this range. In the high discharge ratio of more than 80%, discharge potential decreased monotonously and finally the reduction of propylene carbonate started.

$(C_2F)_n$ electrode has a higher discharge potential than $(CF)_n$ electrode when they are prepared by direct fluorination of the same carbon. As can be seen in Fig. 1-2, $(C_2F)_n$ has a smaller overpotential than that of $(CF)_n$ while OCV's are nearly the same.

4-2 Analysis of polarization decay curve

Figure 2-2 shows potential-$\ln\sqrt{t}$ plots of polarization decay curves of graphite fluoride electrode after 25% discharge. As can be expected from eq. 2-7, the middle parts

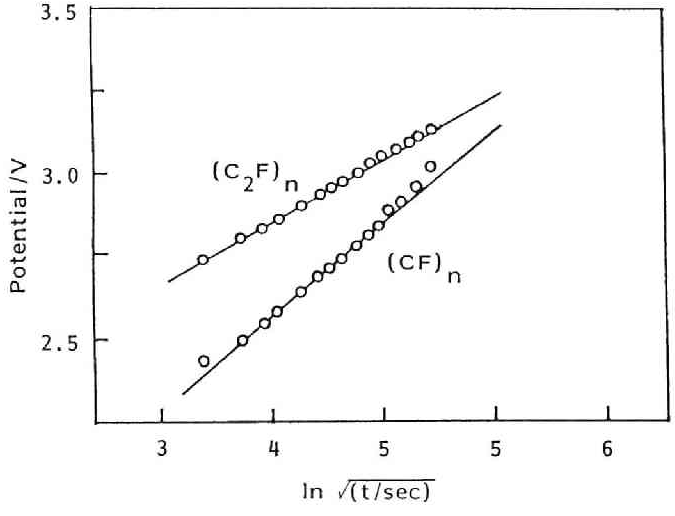

Fig. 2-2 Cathode potential-ln$\sqrt{t}$ plots of graphite fluoride electrodes at 25% discharge(25°C)

of the plots for both $(CF)_n$ and $(C_2F)_n$ gave straight lines. The deviations from the straight line for small and large t values are due to the approximations in the initial condition and semi-infinite boundary condition set up to derive eq. 2-7, respectively. The values of ln a/ln C calculated from the slope of potential-ln $\sqrt{t}$ plots at various discharge ratios are shown in Fig. 2-3. In the first region less than 20% of discharge, ln a/ln C values gradually increased. In the second region from 20 to 80% of discharge, they indicated constant values. In the third region more than 80%, potential-ln $\sqrt{t}$ plots did not give straight lines, so the ln a/ln C values were unable to be estimated. The first region is discharge of the edge part of the graphite fluoride crystallite mainly composed of terminal groups such as CF_2 and CF_3, successively followed by the growth of diffusion layer of GIC. The change in the ln a/ln C values in this range coincides with that expected from thermodynamics, $\lim_{C\to 0}$ ln a/ln C = 1. The second

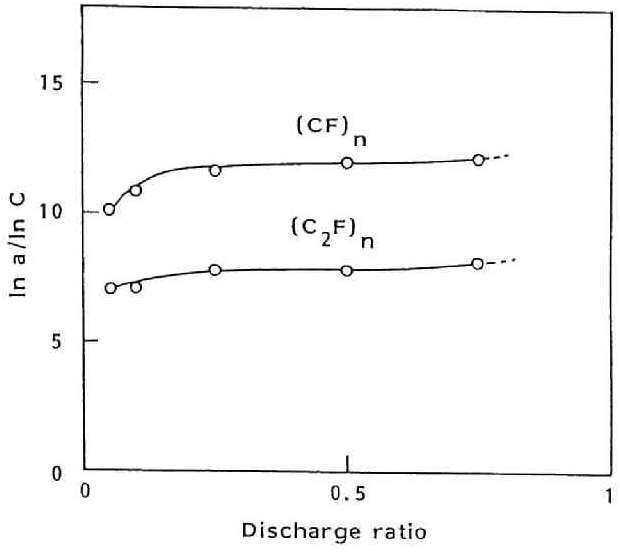

Fig. 2-3 The ln a/ln C value as a function of discharge ratio of graphite fluoride electrodes(25°C)

region is discharge of the bulk of the crystallite, which proceeds heterogeneously along ab-axis by renewing the electrode surface according to eq. 1-5. In the third region, undischarged crystallite becomes small, which causes the increase of overpotential and reduction of the solvents begins as a side reaction.

For the second region where ln a/ln C has a constant value, W was obtained to be 12 for $(CF)_n$ and 8 for $(C_2F)_n$. The smaller value of W for $(C_2F)_n$ than that of $(CF)_n$ suggests that electrons are more concentrated and localized in GIC phase(3). From eq. 2-3, the diffusion of lithium ions are enhanced by 12 and 8 times as those of neutral species, respectively, due to the minus-charged atmosphere around lithium ions. This effect is explained to be caused by the promotion of lithium ion diffusion by the local field arising between lithium ion and electron with a

much higher mobility preceding ahead of lithium ion(3). By pouring lithium ions and electrons in graphite fluoride, covalent bond between fluorine and carbon atoms increase its ionicity and trans-linked cyclohexane carbon array recovers the planar graphitic structure. It has been already suggested by ESCA measurements of discharge products that the bonding between fluorine and carbon is semi-ionic in this phase(4, 5). Both in $(CF)_n$ and $(C_2F)_n$, fluorine atoms are covalently bonded to tertiary carbon atoms, and electrophilicities are regarded as the same. However, the recent investigation with ^{19}F-NMR measurements has shown the existence of a small amount of fluorine species weakly bonded to residual graphitic carbon layers in $(C_2F)_n$ (See Chapter 3). If they have much higher electrophilicity than the covalently bonded, average electron share per one fluorine atom would be larger. With increasing concentration of fluorine species having high electrophilicity in the diffusion layer, the electrons are localized and concentrated in GIC phase, which decreases the value of W. However, at the same time, the thickness of diffusion layer formed on the surface of $(C_2F)_n$ decreases more than that of $(CF)_n$, namely, a thinner diffusion layer is established by fast disproportionation of GIC phase in the case of $(C_2F)_n$ where averagely more polarized fluorine species are easily combined with the lithium ions. As will be discussed in Chapter 3, the concentration decrease of the weakly bonded fluorine in $(C_2F)_n$ by the heat treatment in F_2 atmosphere at high temperatures causes the increase of overpotential. This effect would be important compared with the enhancement of lithium ion diffusion coefficient.

4-3 Chronoamperometry

Figure 2-4 shows $i - 1/\sqrt{t}$ plots of graphite fluoride electrode obtained by the potential step method. To avoid the effect of disproportionation reaction, the potential was

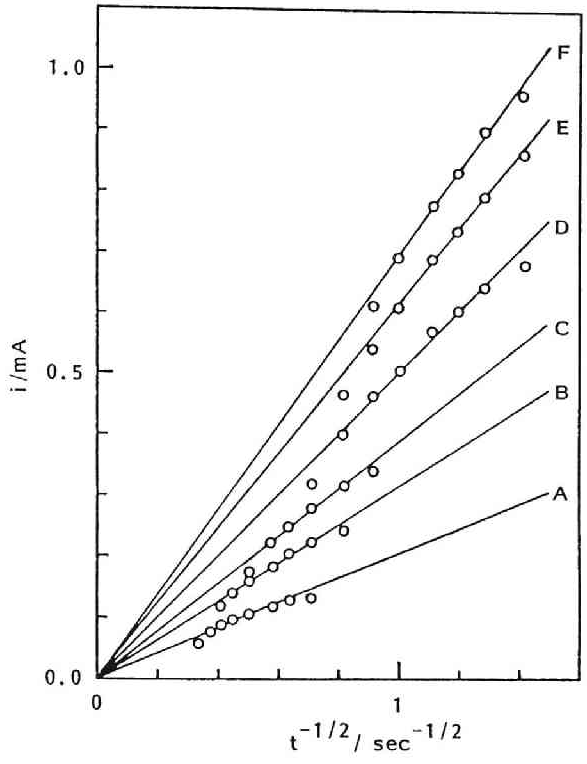

Fig. 2-4 Cathodic current-$t^{-1/2}$ plots of graphite fluoride electrodes using potential step technique
A: $(CF)_n$, 0°C, B: $(CF)_n$, 25°C, C: $(CF)_n$, 43°C, D: $(C_2F)_n$, 0°C, E: $(C_2F)_n$, 25°C, F: $(C_2F)_n$, 43°C

stepped so as not to let flow a steady current to the end. A region where plots are on the straight line crossing the origin exists at every temperature examined for both $(CF)_n$ and $(C_2F)_n$. A deviation from the straight line at small t values is because of the boundary condition set up to derive eq. 2-9. According to eq. 2-9, at t=0, just after the

Table 2-1 D/L^2 values for lithium ion diffusion in graphite fluoride electrode

Temperature/°C	$DL^{-2} \times 10^2/sec^{-1}$	
	$(CF)_n$	$(C_2F)_n$
0	4.9	19.6
25	8.3	25.7
43	13.1	29.7

potential step, current is infinite, however actual current is limited. A deviation at large t values is caused from the invalidity of the condition, $t << L^2/D$, in eq. 2-10.

From eq. 2-10, the slope of the straight line in Fig. 2-4 corresponds to the value of $QD^{1/2}/L\pi^{1/2}$ where Q is measurable by the graphical integration of i-t curve. Results are listed in Table 2-1. The larger D and the smaller L, the easier the lithium ion transfer in GIC phase. So the value of D/L^2 having the dimension of frequency indicates the degree for lithium ion transferability. As can be seen from eq. 2-3, the larger the self-diffusion coefficient, D^* and thermodynamic factor, W, the larger the diffusion coefficient, D.

^{7}Li-wideline-NMR measurement of the discharge products has been performed for the determination of the absolute values of D and L. In this method, temperature dependence of the peak width is measured to determine the hopping rate or self diffusion coefficient, D^*, of lithium nuclei, which provides the absolute D value from eq. 2-3. Unfortunately, the absorptions by lithium in LiF and lithium ion in the electrolyte masked that of lithium in GIC diffusion layer. The thickness of diffusion layer of this

electrode is too thin to be detected by such a measurement, differently from those making homogeneous phase composed of lithium and host material.

The difference in D^* would be due to the difference in the C-axis thickness of the crystallite because the intercalation of a large solvated lithium ion needs expansion of host graphite fluoride layers along C axis(See Chapter 3). However, even if the D^* of $(C_2F)_n$ is larger than that of $(CF)_n$, it cannot be decided that D of $(C_2F)_n$ is larger than that of $(CF)_n$, because the enhancement factor, W of $(CF)_n$ is 1.5 times than that of $(C_2F)_n$. The difference in the thickness of diffusion layer between $(CF)_n$ and $(C_2F)_n$ was discussed above. The faster disproportionation of the diffusion layer provides facilitation of lithium ion transfer in it in the case of $(C_2F)_n$. The contribution of the latter would be larger than the effect of enhancement of lithium ion self-diffusion to the difference in overpotentials between $(CF)_n$ and $(C_2F)_n$.

4-4 Activation energy for lithium ion diffusion

Temperature dependence of diffusion coefficient is expressed by Arrhenius equation,

$$D = D_0 \exp(-Ea/RT) \qquad [2\text{-}12]$$

where D_0 is a frequency factor and E_a is activation energy of diffusion. From eq. 2-12,

$$\ln(QD^{1/2}/L\pi^{1/2}) = -Ea/2R \cdot 1/T + \ln(QD_0^{1/2}/L\pi^{1/2}) \qquad [2\text{-}13]$$

Figure 2-5 shows $\ln(QD^{1/2}/L\pi^{1/2})$ - 1/T plots. Activation energies calculated from the slope of the plots were 5.0 and 3.2 $kcalmol^{-1}$ for $(CF)_n$ and $(C_2F)_n$, respectively, which are reasonable values for diffusion process.

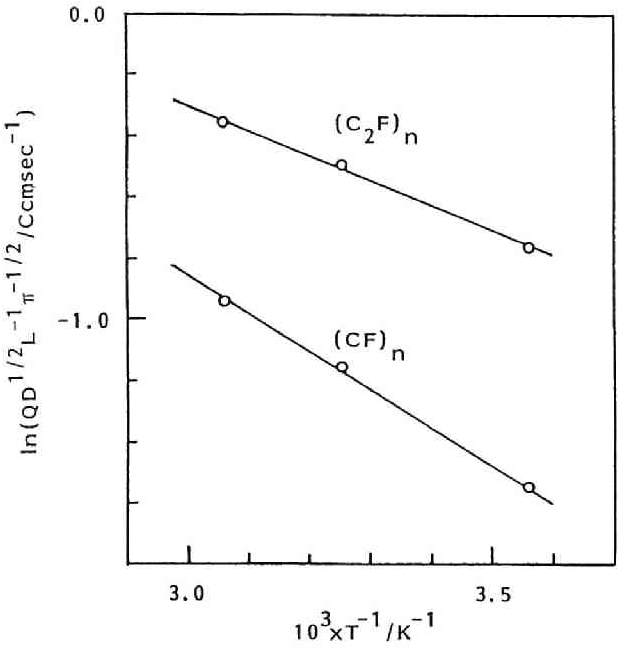

Fig. 2-5 Arrhenius plots of diffusion coefficients of lithium ion in graphite fluoride electrodes

5. SUMMARY

(1) Cathode overpotentials of graphite fluoride electrodes is caused by the delay of lithium ion transfer in the thin diffusion layer composed of discharge products.

(2) The higher discharge potential of $(C_2F)_n$ electrode than that of $(CF)_n$ is due to the difference in the cathode overpotentials.

(3) Two factors must be taken into account for the difference in the cathode overpotentials between $(CF)_n$ and $(C_2F)_n$ electrodes. One is the difference in the diffusion coefficient, and the other is that in the thickness of diffusion layer. The contribution of the latter would be larger than the former.

(4) Activation energy for the lithium ion diffusion were 5.0 for $(CF)_n$ and 3.2 $kcalmol^{-1}$ for $(C_2F)_n$, respectively.

REFERENCES

[1] C. Wagner, J. Chem. Phys., 21, 1819(1953).

[2] M. S. Whittingham, Prog. Solid St. Chem., 12, 41 (1978).

[3] W. Weppner and R. A. Huggins, J. Electrochem. Soc., 124, 1569(1977).

[4] N. Watanabe and K. Morigaki, Denki Kagaku, 47, 174 (1979).

[5] H. Touhara, H. Fujimoto, N. Watanabe and A. Tressaud, Solid State Ionics, 14, 163(1984).

---

1 cal = 4.184 J.

Chapter 3

THE RELATION BETWEEN THE CATHODE OVERPOTENTIAL AND CRYSTALLINITY OF GRAPHITE FLUORIDES

1. INTRODUCTION

Graphite fluorides are obtained in the form of a paracrystallite by direct fluorination of carbon materials at high temperatures. For example, when natural graphite is used as a starting material, $(CF)_n$ is formed around 600°C, while $(C_2F)_n$ is prepared at lower temperatures of 350°-400°C. With increasing fluorination temperature, the composition changes from $(C_2F)_n$ to $(CF)_n$ via their mixture, in which $(CF)_n$ content increases with increasing temperature. It is noted that $(C_2F)_n$ is prepared only by a relatively low temperature fluorination of a highly crystallized graphite, such as natural graphite or graphitized petroleum coke(1). The carbon layers of graphite fluoride consist of an infinite array of trans-linked cyclohexane chairs without aromatic nature. Both in $(CF)_n$ and $(C_2F)_n$, carbon atom with sp^3-hybridized orbital is covalently bonded to fluorine. $(CF)_n$ is regarded as a first stage compound, whereas $(C_2F)_n$ is of the second stage, the stucture of which has been recently investigated in detail(2).

In Chapter 2, it has been revealed that a relatively large overpotential of the graphite fluoride cathode is caused by the delay of lithium ion transfer in the diffusion layer consisting of the ternary intercalation compound of graphite. This chapter is concerned with the relation between the cathode overpotentials and crystallinity of

---

J. Electrochem. Soc., 131, 1980(1984).
Denki Kagaku, 51, 183(1983).

$(CF)_n$ and $(C_2F)_n$. The overpotentials are discussed on the basis of the results obtained by X-ray diffraction, ^{19}F-NMR and ESR measurements. Additionally, the effect of the solvents intercalated with a lithium ion on the discharge characteristics will be discussed.

2. Experimental

$(CF)_n$ and $(C_2F)_n$-type graphite fluorides were prepared by fluorination of Madagascar natural graphite, petroleum coke(original and Heat-treated at 2800°C), vapor-grown carbon fiber(heat-treated at 3000°C) and exfoliated graphite in fluorine gas of 1 atm at temperatures between 290°-600°C. Some of $(C_2F)_n$-type graphite fluorides were prepared via graphite intercalation compound of fluorine as will be discussed in Chapter 4. Synthetic conditions are listed in Table 3-1.

Sample L was heat-treated in fluorine gas of 1 atm at, 400°, 500°, 550°, and 600°C for 24h to investigate the heat-treatment effect on $(C_2F)_n$. In addition to the heat-treatment in fluorine atmosphere, treatment in vacuo at 400°C was also performed for comparison.

The prepared samples were analysed by means of elemental analysis, X-ray diffractometry, ^{19}F-NMR and ESR spectroscopies. NMR measurements were made using a Crossed Coil NMR Spectrometer(Varian WL 109) with scanning of the magnetic field at a fixed radio frequency of 15 MHz. ESR measurements were carried out by the aid of Nihon Denshi, JES-3BX with scanning of the magnetic field at a fixed radio frequency of 9.4 GHz(X-band).

Discharge of graphite fluorides was performed at a fixed current density of 0.5 $mAcm^{-2}$. The polarization curves were also obtained in the range of 10^{-7}-10^{-3} Acm^{-2}. Preparation of electrolyte solutions, electrodes and cell assembly were the same as in Chapter 1.

Table 3-1 Synthetic conditions of graphite fluoride

Samples	Starting carbon	Reaction temp./°C	Reaction time/h	F/C	Notes
A	Madagascar natural graphite	590	28	1.01	$(CF)_n$-type
B	Petroleum coke heat-treated at 2800°C	600	11	1.10	$(CF)_n$-type
C	Petroleum coke heat-treated at 2800°C	510	11	0.99	$(CF)_n$-type
D	Exfoliated graphite	590	11	1.00	$(CF)_n$-type
E	Non-heat-treated petroleum coke	420	7	1.11	$(CF)_n$-type
F	Non-heat-treated petroleum coke	360	7	1.13	$(CF)_n$-type
G	Non-heat-treated petroleum coke	340	9	1.10	$(CF)_n$-type
H	Non-heat-treated petroleum coke	290	21	1.14	$(CF)_n$-type
I	-----	---	--	1.05	$(CF)_n$-type commercially available
J	-----	---	--	1.06	$(CF)_n$-type commercially available
K	Madagascar natural graphite	390	168	0.61	$(C_2F)_n$ -type
L	Madagascar natural graphite	350	504	0.66	$(C_2F)_n$ -type
M*	Madagascar natural graphite	340	97	0.58	$(C_2F)_n$ -type
N*	Madagascar natural graphite	390	23	0.63	$(C_2F)_n$ -type
O*	Madagascar natural graphite	340	50	0.59	$(C_2F)_n$ -type
P	Vapor-grown carbon fiber heat-treated at 3000°C	370	50	0.59	$(C_2F)_n$ -type

* Prepared via GIC(See Chapter 4).

3. RESULTS AND DISCUSSION

3-1 The relation between crystallinity and cathode overpotential of graphite fluorides

Figure 3-1 shows the plots of the cathode overpotentials of $(CF)_n$ at 25% discharge against the interlayer spacing, $d_{(002)}$ and half-width, $\beta_{(002)}$ of diffraction line. The overpotential decreased with increasing $d_{(002)}$ and $\beta_{(002)}$. Since the thickness of monolayer of graphite

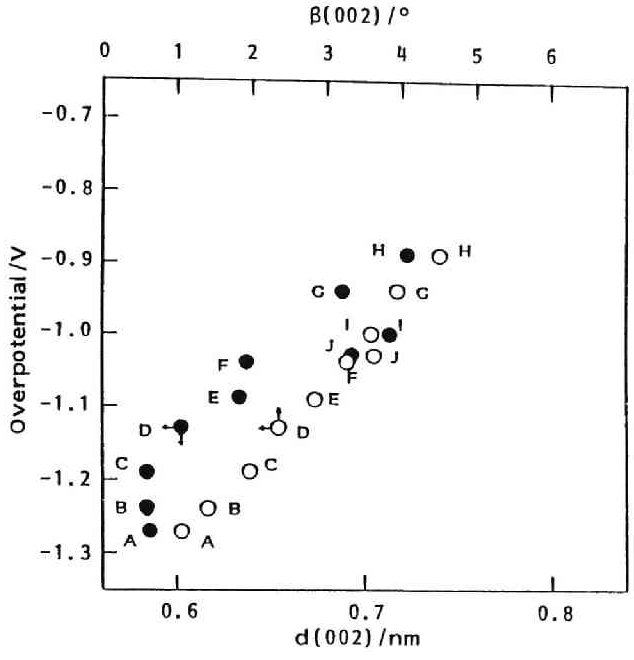

Fig. 3-1 Cathode overpotentials of $(CF)_n$ electrodes as a function of d(002) and β(002) 0.5mAcm^{-2}, at 25% discharge.

fluoride is the same among all the samples, the space between monolayers increases with increasing $d_{(002)}$. The half-width, $\beta_{(002)}$ is inversely proportional to the thickness of the graphite fluoride crystallite along C axis. As the crystallite size and $d_{(002)}$ spacing of graphite fluoride strongly depend on the crystallinity of a starting carbon material, these factors can be controlled by choosing the starting carbon material as well as reaction temperature. It has already been pointed out in Chapter 2 that the overpotential of graphite fluoride electrode is caused by the delay of the transfer of solvated lithium ion in the diffusion layer. The increase in the space between monolayers of graphite fluoride with increasing $d_{(002)}$, and the decrease in thickness of the crystallite along C axis

would facilitate the transfer of lithium ion in the diffusion layer on the discharge process(Fig. 3-2).

It was confirmed prior to this experiment that the overpotential was independent of the particle size of graphite fluoride as shown in Fig. 3-3 where a comparison is made among the overpotentials of $(CF)_n$ prepared from Madagascar natural graphite with different particle sizes, at the current density of 0.5 $mAcm^{-2}$. Futhermore discharge behaviors of two types of mixtures of $(CF)_n$ and $(C_2F)_n$ were markedly different with each other as shown in Fig. 3-4. Fig. 3-4(A) shows the discharge curves of the mixtures of separately prepared $(CF)_n$ and $(C_2F)_n$ with several mixing ratios. $(C_2F)_n$ with smaller cathode overpotential than that of $(CF)_n$ discharged first, then followed by the discharge of $(CF)_n$ at every mixing ratio. This is obvious also from the X-ray diffraction patterns of the discharge products shown in Fig. 3-5(A) where (002) diffraction line of $(C_2F)_n$ disappeared first while that of $(CF)_n$ almost unchanged until the end of the discharge of $(C_2F)_n$. Fig. 3-4(B) is the discharge curves of $(CF_x)_n$, x being changed by controlling the fluorination temperature. Of course these are also the mixtures of $(CF)_n$ and $(C_2F)_n$, however, mixing occurs in the host graphite crystallite on the fluorination process. In this case, discharges of $(CF)_n$ and $(C_2F)_n$ parts proceed simultanously to give a flat and averaged discharge potential which depends on the F/C ratio of the sample. The X-ray diffraction patterns shown in Fig. 3-5(B) also indicate that neither of their peaks have disappeared at the early stage of discharge, which means the discharge of both graphite fluorides occurs at the same time. From these results,it can be concluded that the discharge reaction is not determined by the transfer of lithium ion out of the particles but by that at the bulk of the particles of graphite fluoride(Fig. 3-2).

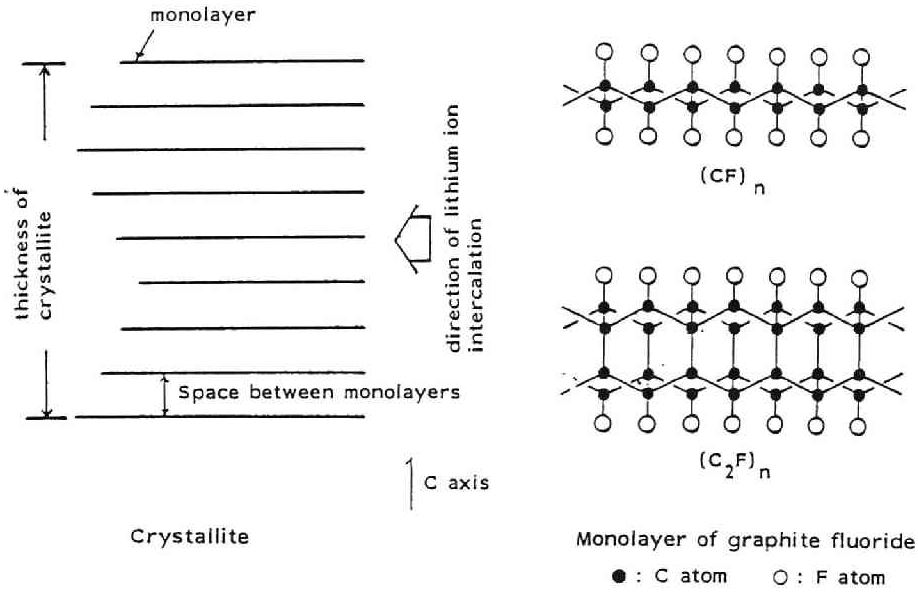

Fig. 3-2 Schematic illustrations of graphite fluoride crystallites

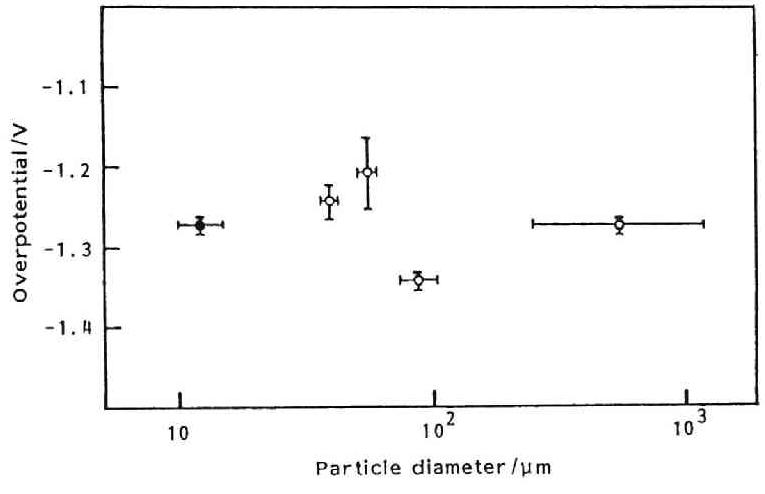

Fig. 3-3 The relation between overpotential and particle size of graphitized carbon used for preparing $(CF)_n$ *

○: Madagascar natural graphite
●: Petroleum coke graphitized at 2800°C

* Galvanostatic discharge ($0.5 mA cm^{-2}$).
d(002) : 0.59 nm β(002) : $1.4 \pm 0.2°$

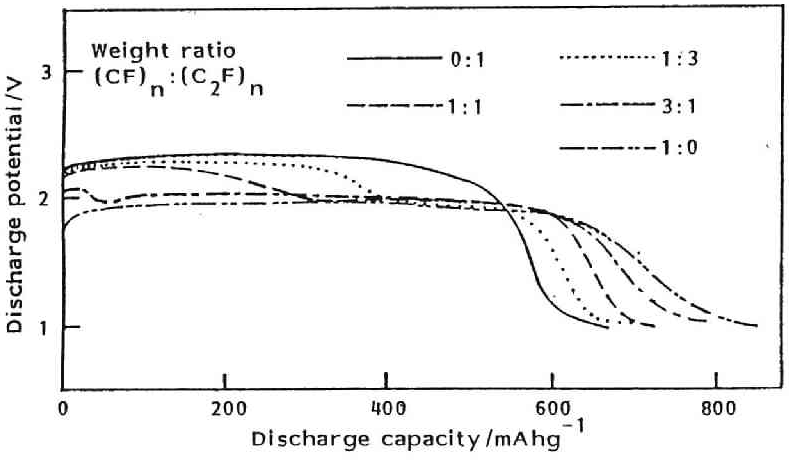

(A) Mixed electrodes of $(CF)_n$ and $(C_2F)_n$

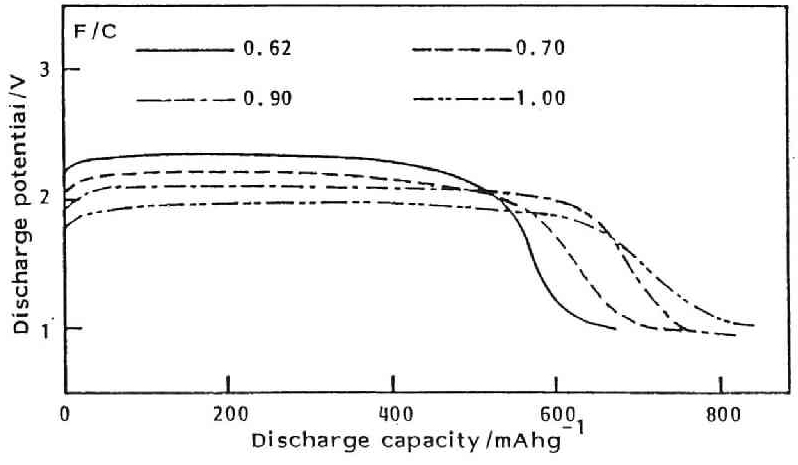

(B) Electrodes of graphite fluorides with various F/C ratios

Fig. 3-4 Discharge curves of the mixed electrodes of $(CF)_n$ and $(C_2F)_n$

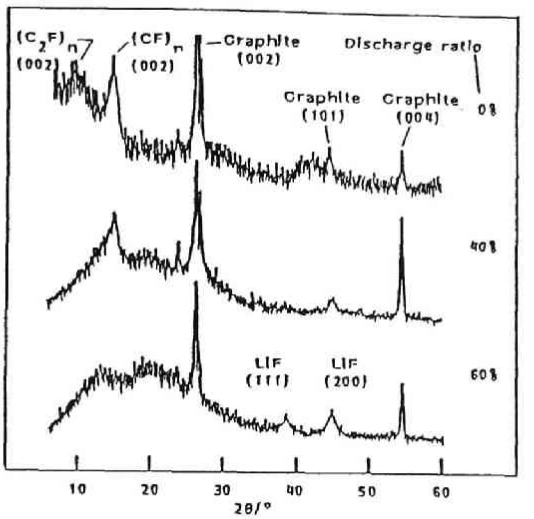

(A) $CF_{0.62}$: $CF_{1.00}$: Exfoliated graphite
= 1 : 1 : 2(weight ratio)

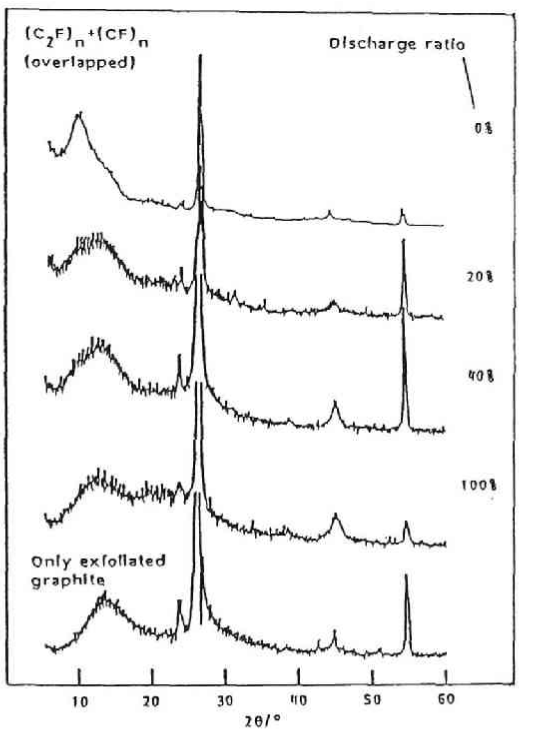

(B) $CF_{0.70}$: Exfoliated graphite = 1 : 1

Fig. 3-5 X-ray diffraction patterns of the discharge products in the mixed electrodes of $(CF)_n$ and $(C_2F)_n$

Unlike $(CF)_n$-type, it is difficult to prepare $(C_2F)_n$-type graphite fluorides with large differences in crystallinity, $d_{(002)}$ and $\beta_{(002)}$, because starting carbon materials and reaction temperature are limited in this case. $(C_2F)_n$ can be prepared only from a highly graphitized carbon material such as natural graphite at 350°-400°C(1). Ungraphitized petroleum coke with a low crystallinity gives only $(CF)_n$ at any temperature. For every $(C_2F)_n$ prepared, the overpotential at a current density of 0.5 $mA\,cm^{-2}$ was about 0.9 V, which corresponded to the minimum value for that of $(CF)_n$.

Figure 3-6 shows the typical discharge curves of $(CF)_n$ and $(C_2F)_n$. The flatness of discharge potential for $(CF)_n$ was improved with increasing crystallinity of the sample while the discharge potential decreased. In other words, the height and flatness of discharge potential are compensative with each other. Even for $(CF)_n$, the overpotential was decreased approaching to that of $(C_2F)_n$ by choosing a carbon with low crystallinity as a starting material and by fluorinating it at a low temperature, however, the flatness of discharge potential was inferior.

3-2 The effects of the heat-treatment of $(C_2F)_n$ on the discharge characteristics and structure

Figure 3-7 and Table 3-2 show the discharge characteristics of heat-treated $(C_2F)_n$ in lithium battery. With increasing the heat-treatment temperature,the discharge potential decreased and the flatness of discharge potential was improved at the beginning of discharge. The effects of the heat-treatment at 400°C on discharge characteristics were scarcely observed. As can be seen in Table 3-2, the decrease of discharge potential is caused by the increase of overpotential rather than the decrease of open-circuit voltage. In the present work, as described below, the improvement of crystallinity of $(C_2F)_n$ by the heat-

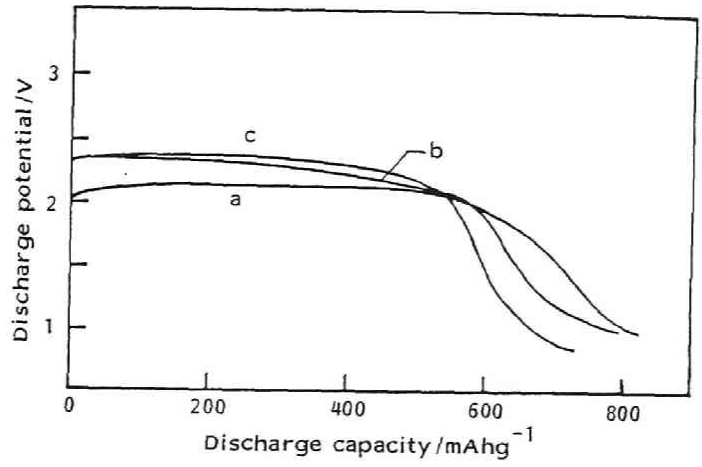

Fig. 3-6 Discharge curves of graphite fluorides ($0.5\ mAcm^{-2}$)
a: $(CF)_n$ (sample A), b: $(CF)_n$ (sample E)
c: $(C_2F)_n$ (sample K)

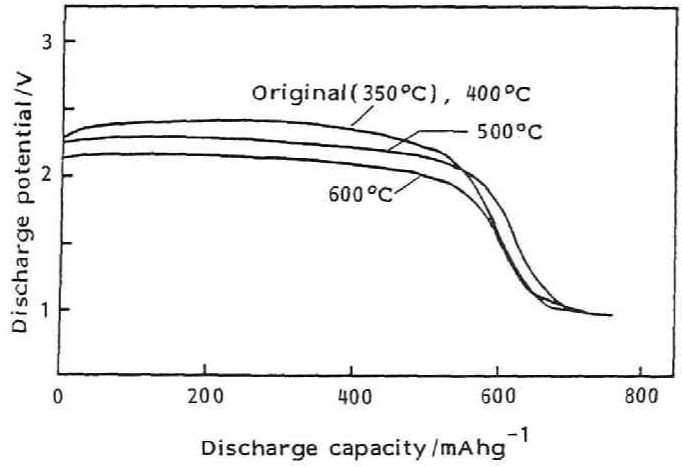

Fig. 3-7 Effects of heat treatment on discharge characteristics of $CF_{0.66}$ (sample L, $0.5\ mAcm^{-2}$)

Table 3-2 Discharge characteristics of heat-treated $CF_{0.66}$ prepared from natural graphite(Sample L)

Temperature /°C	OCV /V	Discharge potential /V	Overpotential /V	Discharge capacity /mAhg^{-1}
350	3.30	2.41	0.89	690
400	3.28	2.38	0.90	730
500	3.26	2.28	0.98	720
600	3.24	2.14	1.10	710

treatment was not found as far as the analysis by X-ray diffractometry was concerned. Nevertheless, the overpotential was fairly changed by the heat-treatment.

With increasing temperature of the heat-treatment in fluorine gas, the color of $(C_2F)_n$ gradually changed from black to white, while the weight of the sample scarcely changed, except for that heat-treated at 600°C, whose weight decreased by 1-2%. The $d_{(002)}$ and $\beta_{(002)}$ were also unchanged by the heat-treatment for every sample, which indicates that the improvement of crystallinity was not achieved by this treatment. The F/C ratio, $d_{(002)}$ and $\beta_{(002)}$ were 0.66 ± 0.02, 0.81 ± 0.01 nm and 3.2 ± 0.2°, respectively.

Figure 3-8 shows ^{19}F-NMR spectra of $(C_2F)_n$, where two kinds of resonance absorptions were obsereved. One was very broad with peak-to-peak width, $\Delta H'$ of 9.0 ± 0.1 G, and the other was sharp one with $\Delta H'$ of 1.5 ± 0.1 G. No change of the line width was observed by the heat-treatment. Differential gradient method showed that the narrow absorption line was Lorentzian, which is related to homogeneous system where the energy absorbed from oscillating magnetic field is distributed so that the spin system

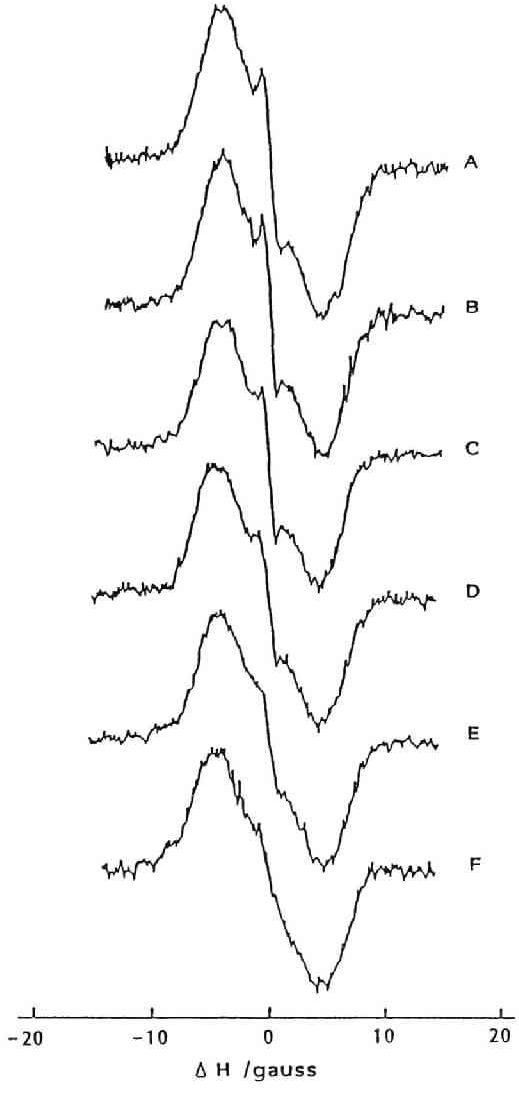

Fig. 3-8 ^{19}F-NMR spectra of heat-treated $CF_{0.66}$(sample L)

A:Original(prepared at 350°C),
B:400°C in F_2, C:400°C in vacuo,
D:500°C in F_2, E:550°C in F_2,
F:600°C in F_2.
ν=15 MHz, H_0=3750 G, MA=0.5 G

may maintain the thermal equilibrium through the resonance process. The narrow line width would correspond to motional narrowing, which means that fluorine atoms make weak chemical bonds with carbon atoms, therefore having higher activity than those covalently bonded. This absorption line decreased as the heat-treatment temperature increased and almost disappeared at 600°C. A slight decrease of the open-circuit voltage, shown in Table 3-2, might be caused by the decrease of these fluorines weakly bonded with carbon atoms. The decrease of absorption intensity by the heat-treatment was slightly larger in vacuo at 400°C than in fluorine gas at the same temperature. The broad absorption line was approximately Gaussian, where each spin is situated in different local fields, which causes the line broadening. By taking the line width and peak intensity into consideration, this spin component is attributable to the major part of fluorine atoms in graphite fluoride, namely, fluorine atoms covalently bonded to carbon atoms. Consequently, there are two kinds of fluorine species in $(C_2F)_n$. For $(CF)_n$ prepared from highly graphitized carbon at around 600°C, only one broad absorption line was observed with the same $\Delta H'$ as that of $(C_2F)_n$, which means that $(CF)_n$ has only a covalent bond between fluorine and carbon atoms.

Fig. 3-9 shows the results of ESR measuremnts. ESR spectra of $(C_2F)_n$ gave a single peak with a constant g value of 2.004 having no dependence on the heat-treatment temperature. From the g value, the radicals observed are reasonably ascribed to carbon. As the g value was also 2.004 in case of $(CF)_n$, the radicals are the same kind, even though the intensity of the signal was much smaller than that of $(C_2F)_n$. As shown in Fig. 3-9, the peak-to-peak width, $\Delta H'$, increased rapidly with increasing heat-treatment temperature, however, gradually increased above 500°C. Futhermore, the differential gradient method showed that the type of the absorption line was changed from

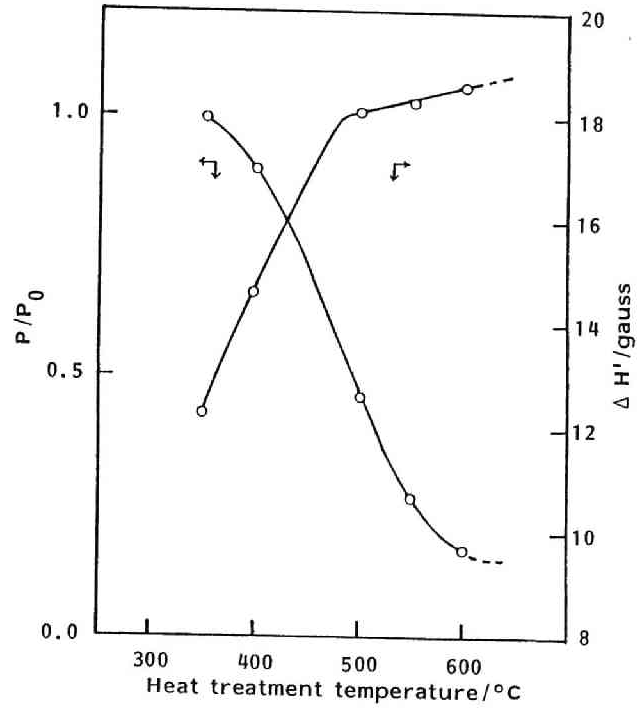

Fig. 3-9 Change in ESR spectra of $CF_{0.66}$ (sample L) by heat treatment

ΔH': Peak-to-peak width
P : Absorption intensity $\times(\Delta H')^2$
P_0: P of original one

Lorentzian to Gaussian with increasing heat-treatment temperature. The P value(the product of the peak-to-peak height with the square of the line width of a differential absorption line) approximately corresponding to radical concentration decreased monotonously with increasing heat-treatment temperature.

From the above results, the following discussion is derived. The ESR measurement indicates that $(C_2F)_n$ contains a small amount of unreacted carbon which is so randomly distributed as being unable to be detected by X-ray diffractometry and elemental analysis. The presence of unreacted carbon was recently confirmed by a high resolution

electron microscope(3). It is regarded as a kind of defect which would be present in the form of polynuclear aromatic carbon rings in $(C_2F)_n$. This carbon produces carbon radicals by making covalent bonds partially with fluorine atoms or the cleavage of double bond. The black color of $(C_2F)_n$ is therefore caused by these defects. Namely, the defects in the $(C_2F)_n$ heat-treated at low temperatures have fairly long conjugated π systems, so the π- π^* transition energy is in the range of visible lights. The n-π^* transition by the delocalized radicals is also in this range. The fluorine species giving a narrow absorption line detected in ^{19}F-NMR measurements have weak chemical bonds with the unreacted carbon. With increasing heat-treatment temperature, the double bonds are cleaved to make covalent bonds with mobile fluorine species, which causes the decrease and localization of radicals. Consequently, the broadening of the line width and the transformation from Lorentzian to Gaussian are observed in ESR spectra. At the same time, the intensity of the narrow-width line is lowered in NMR spectra. In this way, the defect concentration decreases with increasing heat-treatment temperature. By the destruction of the conjugated π systems, the light absorption shifts out of the visible light range and the color of $(C_2F)_n$ is changed to white. The difference between the heat-treatments in fluorine gas and in vacuo was not so remarkable at 400°C. The interaction between fluorine gas and the carbon radicals inside the graphite fluoride(4) would not be so strong at such a temperature. It is interesting to estimate the absolute radical concentration in graphite fluoride. The comparison was made using carbonized dextrose as a standard sample whose spin density has been already known(5). According to this method, the order of radical concentration in $(C_2F)_n$ was 10^{20}-10^{21} spins/g, which means that it has one radical per several tens to several hundreds of carbon atoms. The

radical concentration in $(CF)_n$ was less than tenth part of that in $(C_2F)_n$ heat-treated at 600°C.

The effects of the defects in $(C_2F)_n$ on the discharge characteristics can be described as follows. The defects are in the form of polynuclear aromatic carbon rings in $(C_2F)_n$. Around these defects, the chemical bond between carbon and fluorine atoms would be so weak that the ternary graphite intercalation compounds, $C_2F^- \cdot Li^+ \cdot zS$, produced by the discharge reaction would be more easily decomposed to carbon, lithium fluoride, and solvent molecules, which would decrease the thickness of the lithium ion diffusion layer at the surface of graphite fluoride. Such defects in $(C_2F)_n$ are considered to be a kind of short circuiting path that decreases the overpotential by decreasing the averaged thickness of the lithium ion diffusion layer composed of GIC as discussed in Chapter 2. For $(CF)_n$, this kind of effect is much smaller than in $(C_2F)_n$ because the defect concentration is much lower. The heat-treatment of $(C_2F)_n$ is just the elimination of the defect which lowers the overpotential. The improvement of the flatness of discharge potential would arise from the decrease of the defect concentration inside the graphite fluoride crystallite by the heat-treatment.

3-3 The difference in the discharge performance between $(CF)_n$ and $(C_2F)_n$

Figure 3-10 shows typical cathodic polarization curves of $(CF)_n$(sample A), $(C_2F)_n$, and that heat-treated at 600°C(sample K) at 25% discharge. All the samples were prepared from Madagascar natural graphite. Their open-circuit voltages were almost the same, 3.27 ± 0.02 V at 25% discharge. In every case, the plots of cathode potentials against the logarithms of current densities gave a straight line in the range of less than 10^{-4} Acm^{-2} with a bending point at the current density of 10^{-6} - 10^{-5} Acm^{-2}.

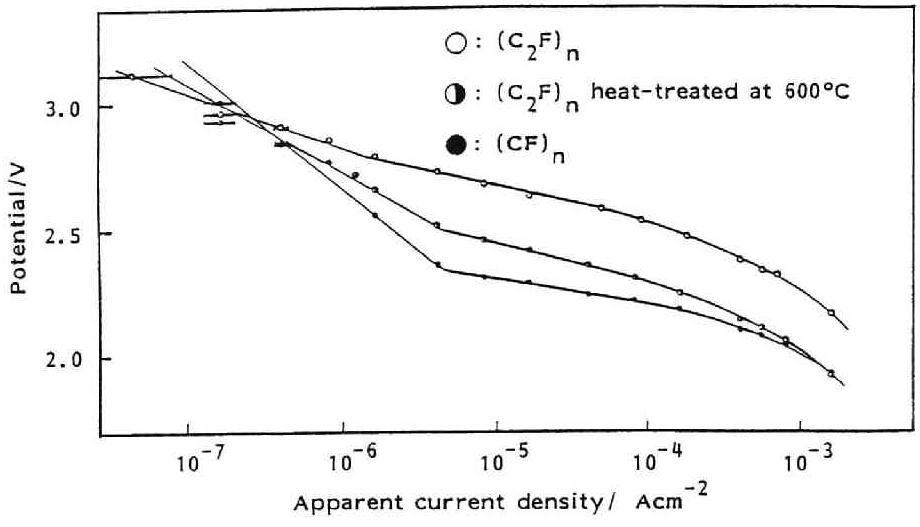

Fig. 3-10 Galvanostatic polarization curves of graphite fluoride electrodes(at 25% discharge)
$(CF)_n$: sample A, $(C_2F)_n$: sample K

However, the current-interrupter method revealed that no activation overpotential was present in this region. It can be said that the rate-determining step of the discharge reaction is the transfer of lithium ion in the ternary phase in the whole region in Fig. 3-10.

Two factors must be taken into consideration to evaluate the difference in discharge potentials between $(CF)_n$(sample A) and $(C_2F)_n$(sample K). One is the thickness of graphite fluoride crystallite along the C axis, discussed above, and the other is the short circuiting paths which arise from the defects in graphite fluoride, also discussed above. The space between monolayers of graphite fluoride was found to be almost the same for both $(CF)_n$ and $(C_2F)_n$ when they were prepared from a highly graphitized carbon material(2). The discharge potential of $(C_2F)_n$ (sample K) was higher by 0.3-0.4 V than that of

$(CF)_n$(sample A) in the range of 5×10^{-6} - 5×10^{-4} Acm^{-2}, being, however, decreased by 0.2 V with heat-treatment at 600°C in fluorine gas. This difference in the discharge potentials between the original and heat-treated $(C_2F)_n$'s is attributed to the decrease in the defect concentration. $(C_2F)_n$ with more short circuiting paths gives the higher discharge potential than the heat-treated one. Consequently, the difference in the discharge potential between $(CF)_n$ and heat-treated $(C_2F)_n$($\leq$ 0.1V) would be mainly due to the difference in the thickness of the crystallite of graphite fluoride along C axis, which was 3 nm for heat-treated $(C_2F)_n$ and 6 nm for $(CF)_n$(sample A) by the approximate calculation from the half-width of (002) diffraction line, $\beta_{(002)}$. The transfer of lithium ion between graphite fluoride layers would be faster in heat-treated $(C_2F)_n$ with the thinner crystallite than in $(CF)_n$ on the discharge process.

3-4 The effects of the electrolyte solvents on the discharge performance of graphite fluoride

Discharge curves of $(CF)_n$ and $(C_2F)_n$ electrodes in several kinds of aprotic organic solvents are shown in Fig. 3-11. In every solvent, the discharge potential of $(C_2F)_n$ electrode is higher by 0.2-0.3 V than that of $(CF)_n$ electrode on galvanostatic discharge of 0.5 $mAcm^{-2}$. The overpotential of $(C_2F)_n$ electrode is lower by 0.2-0.3 V than that of $(CF)_n$ in every solvent because both OCV's are almost the same as shown in Chapter 1. In comparison among four kinds of solvents for both $(CF)_n$ and $(C_2F)_n$ electrodes, more excellent characteristics, namely the more stable and higher discharge potential and higher discharge capacity were found in DMSO, BL, PC and TMS in that order.

Figure 3-12 is the relationship between the overpotential and molar volume of each solvent. The overpotential

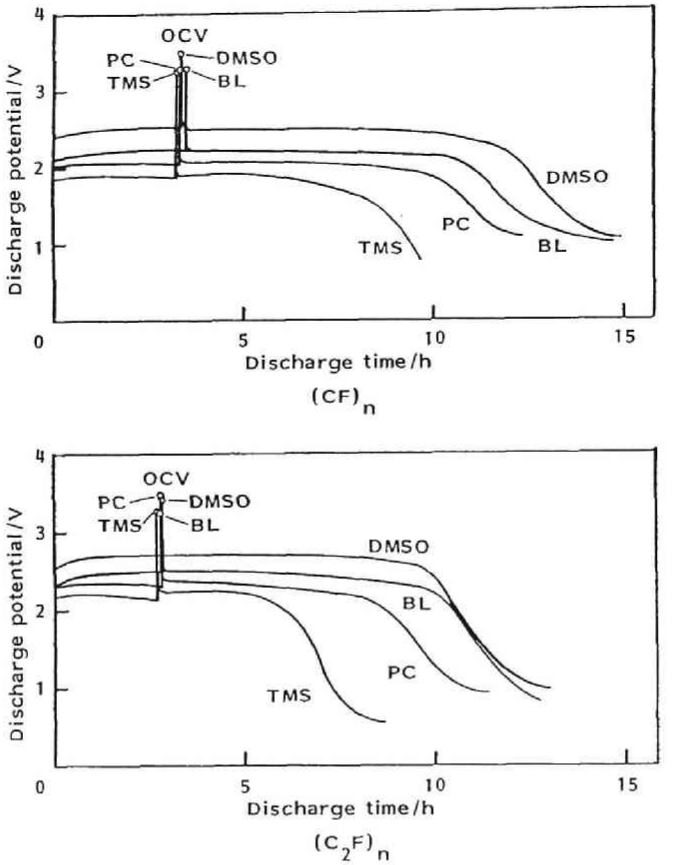

Fig. 3-11 Discharge characteristics of graphite fluoride cathodes in several aprotic solvents($0.5mAcm^{-2}$)

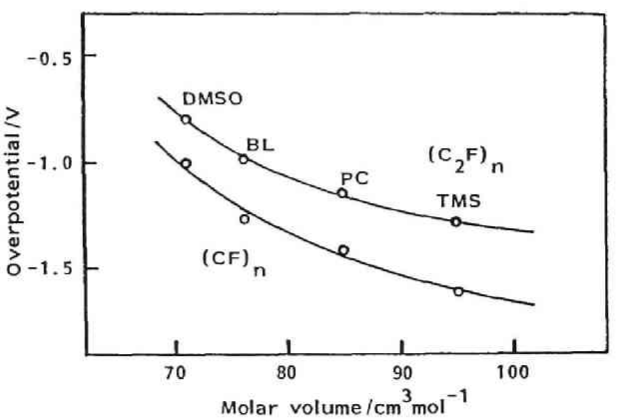

Fig. 3-12 Overpotential of graphite fluoride electrode vs molar volume of solvent

increased with increasing molar volume of the solvent. With respect to the solvents, the size of solvated ion depends on the size of a solvent molecule, solvation number and coordination structure. Figure 3-12 suggests that lithium ions solvated by solvent molecules having smaller alkyl groups can migrate more easily in the diffusion layer of ternary GIC, which leads to the smaller overpotential.

4.SUMMARY

(1) The overpotential of $(CF)_n$ electrode decreased with increasing interlayer spacing and decreasing thickness of the crystallite along the C axis. The diffusion of a large solvated lithium ion needs expansion of host layers of graphite fluoride. A large interlayer spacing and small thickness of the crystallite along C axis facilitates the diffusion of lithium ion.

(2) The overpotential of $(C_2F)_n$ electrode depends on the defect concentration. Defects exist in the form of poly-nuclear aromatic carbon rings where fluorine species are non-covalently bonded which promote the decomposition of the diffusion layer composed of a discharge product and decrease its thickness. Defect concentration decreased by the heat treatment in fluorine atmosphere, which provided the overpotential increase.

(3) The higher discharge potential of $(C_2F)_n$ than that of $(CF)_n$ was mainly attributed to the effect of the defects contained in $(C_2F)_n$.

(4) Aprotic organic solvents by which a lithium ion is solvated also affects the overpotential. The larger the size of the solvent molecule, the larger the observed over-potential. It is due to difference in facility of lithium ion transfer in the diffusion layer.

REFERENCES

[1] Y. Kita, N. Watanabe and Y. Fujii, J. Am. Chem. Soc., 101, 3832(1979).

[2] H. Touhara, K. Kadono and N. Watanabe, Tanso, 117, 98 (1984).

[3] H. Touhara, K. Kadono, M. Endo and N. Watanabe, in "The 10th Annual Meeting of the Carbon Society of Japan," p. 136, Tokyo(1983).

[4] S. Koyama, Ph.D. Thesis, Kyoto University, Kyoto, Japan (1980).

[5] R. H. Hoskins and R. C. Pastor, J. Appl. Phys., 31, 1506(1960).

Chapter 4

DISCHARGE CHARACTERISTICS OF GRAPHITE FLUORIDES PREPARED VIA GRAPHITE INTERCALATION COMPOUNDS

1. INTRODUCTION

Synthesis of graphite fluorides so far has been done by direct fluorination of graphite. Reaction temperature for synthesis of $(CF)_n$ ranges widely from 300°C to 600°C, depending on the crystallinity of pristine graphite as discussed in Chapter 3. Generally the higher the crystallinity of the graphite, the higher reaction temperature is required. Decomposition of $(CF)_n$ to gaseous fluorocarbons occurs as a side reaction, especially when the fluorination of low graphitized carbon is made at relatively high temperatures, which decreases the yield of $(CF)_n$. On the other hand, for preparation of $(C_2F)_n$, the reaction temperature is limited to the range between 350 and 400°C, and the pristine carbon must possess high crystallinity such as that of natural graphite and petroleum cokes graphitized at more than 2800°C. Fluorination at higher temperatures than this causes a significant mixing of $(CF)_n$. Low temperature fluorination can provide a higher yield than that of $(CF)_n$ without decomposition to gaseous fluorocarbons. One of the important problems for $(C_2F)_n$ is that it takes a much longer reaction time than $(CF)_n$. For example, $(CF)_n$ is prepared by fluorinating natural graphite at 600°C for several hours, however, the preparation of $(C_2F)_n$ at 350°C needs as long as three weeks (See Table 3-1).

Recently a new synthetic method of graphite fluorides has been developed via ionic graphite intercalation

---

Electrochim. Acta, 30, 1541(1985).

compounds of fluorine(1). Highly graphitized carbon does not react with fluorine below 300°C, however, fluorine is intercalated into graphite to form an acceptor type of intercalation compound in the presence of metal fluoride at an ambient temperature(1). This ionic graphite intercalation compound decomposes with deintercalation of fluorine to give a graphite exfoliated along the C axis, which can be more easily refluorinated to form graphite fluorides by successive temperature increase in fluorine gas. This method increases the reaction rate of fluorine with graphite from several to several tens times compared with that of direct fluorination of graphite. In the present study, the discharge characteristics of $(CF)_n$ and $(C_2F)_n$ prepared by this method were investigated in comparison with those of graphite fluorides prepared by the conventional method. The heat treatment of $(C_2F)_n$ was carried out at high temperatures under fluorine atmosphere and the effect on the discharge performance was evaluated.

2. EXPERIMENTAL

Madagascar natural graphite(61-74 and 250-850 μm) and petroleum coke graphitized at 2800°C(10-15 μm) were used as pristine graphites. Graphites and commercially available magnesium fluoride powder(purity >98%) were put in a nickel boat without mixing, which was then moved into a nickel reaction tube. The tube was evacuated at 200°C for several hours, and then fluorine gas(purity of 99.4-99.7%) was introduced into the reactor up to 1 atm at ambient temperature. Before introducing fluorine gas, hydrogen fluoride was eliminated by passing through the sodium fluoride column heated at 110°C. After 5-10 h, the temperature was elevated by 3.3 and 17.0°Cmin^{-1} for preparation of $(C_2F)_n$ and $(CF)_n$ respectively, and held for several tens of hours at the terminal temperature to complete the

Table 4-1 Synthetic conditions and analytical data of graphite fluorides

Sample	Starting material	Temp.[1] /°C	Time /hour	X-ray diffraction data β(002)/°	F/C
A1	Madagascar natural graphite(61-74 μm)	340	97.0	3.0	0.58
A2	Madagascar natural graphite(61-74 μm)	340	147.0	2.9	0.63
B	Madagascar natural graphite(61-74 μm)	390	23.0	3.8	0.63
C1	Madagascar natural graphite(61-74 μm)	440	18.5	4.1	0.71
C2	Madagascar natural graphite(61-74 μm)	430	32.0	4.3	0.71
D1	2800°C heat-treated petroleum coke	340	50.0	4.0	0.59
D2	2800°C heat-treated petroleum coke	340	92.0	4.0	0.65
E	2800°C heat-treated petroleum coke	390	23.5	4.5	0.69
F[2]	Madagascar natural graphite(200-830 μm)	430	0.5	3.5	1.01
G[3]	Madagascar natural graphite(61-74 μm)	350	504.0	3.0	0.65
H[3]	Madagascar natural graphite(200-830 μm)	610	18.0	1.6	1.06

1) Samples A-F were prepared via graphite intercalation compounds by temperture increasing method. Temperatures listed here indicate terminal ones.
2) Temperature of this sample was increased at the rate of 17°C/min. The rate of others was 3.3°C/min.
3) Prepared by direct fluorination of graphite.

reaction. The conditions of synthesis are listed in Table 4-1. Some $(C_2F)_n$'s prepared were heat-treated under 1 atm of fluorine atmosphere at various temperatures for one day as shown in Table 4-2.

Discharge experiments were performed in the same manner

Table 4-2 Heat treatment conditions and analytical data of $(C_2F)_n$

Sample	Starting material	Heat treatment temperature/°C[1)]	F/C	X-ray diffraction data β(002)/°
A2	Madagascar natural graphite(61-74 μm)	-	0.63	3.1
A2-400	A2	400	0.67	3.4
A2-500	A2	500	0.68	3.6
A2-600	A2	600	0.70	3.5
C2	Madagascar natural graphite(61-74 μm)		0.71	3.5
C2-500	C2	500	0.70	3.9
C2-600	C2	600	0.69	3.8
D2	2800°C heat-treated petroleum coke	-	0.63	4.0
D2-370	D2	370	0.73	4.5
D2-480	D2	480	0.74	4.8
D2-600	D2	600	0.91	5.3[2)]
G[3)]	Madagascar natural graphite(61-74 μm)	-	0.66	3.2
G-400[3)]	G	400	0.66	3.2
G-500[3)]	G	500	0.66	3.2
G-600[3)]	G	600	0.66	3.2

1) Heat treatments were made in 1 atm of F_2 atmosphere for one days.
2) The (002) peak of this sample was split into two peaks.
3) See Chapter 3.

as shown in Chapter 1. Electrolyte used was 1M lithium perchlorate-propylene carbonate solution. Samples prepared were analysed by means of X-ray diffractometry, wide line NMR spectrometry and ESR spectrometry. Elemental analysis of carbon and fluorine was done at the Laboratory for Organic Elemental Microanalysis of Kyoto University.

3. RESULTS AND DISCUSSION

3-1 Differences of discharge characteristics between graphite fluorides by direct fluorination and those prepared via graphite intercalation compounds of fluorine

$(CF)_n$ prepared via graphite intercalation compound (sample F) possessed a larger half width of 3° in (002) diffraction line than that prepared by direct fluorination, whose half width was 1-2°(sample H) as shown in Table 4-1. Since the thickness of the crystallite along C axis of graphite compounds is inversely proportional to the half width of (002) diffraction line, a larger half width means a smaller thickness of crystallite. On the other hand, $(C_2F)_n$ prepared from natural graphite at 340°C(samples A1 and A2) possesed the same half widths of (002) diffraction lines as that of $(C_2F)_n$ prepared by direct fluorination (sample G). Larger half widths than ca. 3° were observed for $(C_2F)_n$ prepared at higher temperatures than 350°C(samples B, C1, C2) and those prepared from heat-treated petroleum coke (sample D1, D2, E). However, this is due to the mixing of $(CF)_n$ which gives the (002) diffraction line at a higher angle than $(C_2F)_n$, rather than the decrease of crystallite size along the C axis. For the preparation of $(C_2F)_n$, the decrease in crystallite size along the C axis was not attained by exfoliation with this method without a significant mixing of $(CF)_n$. However, for the preparation of $(CF)_n$, a large decrease in crystallite size along the C axis was observed(sample F). The SEM images

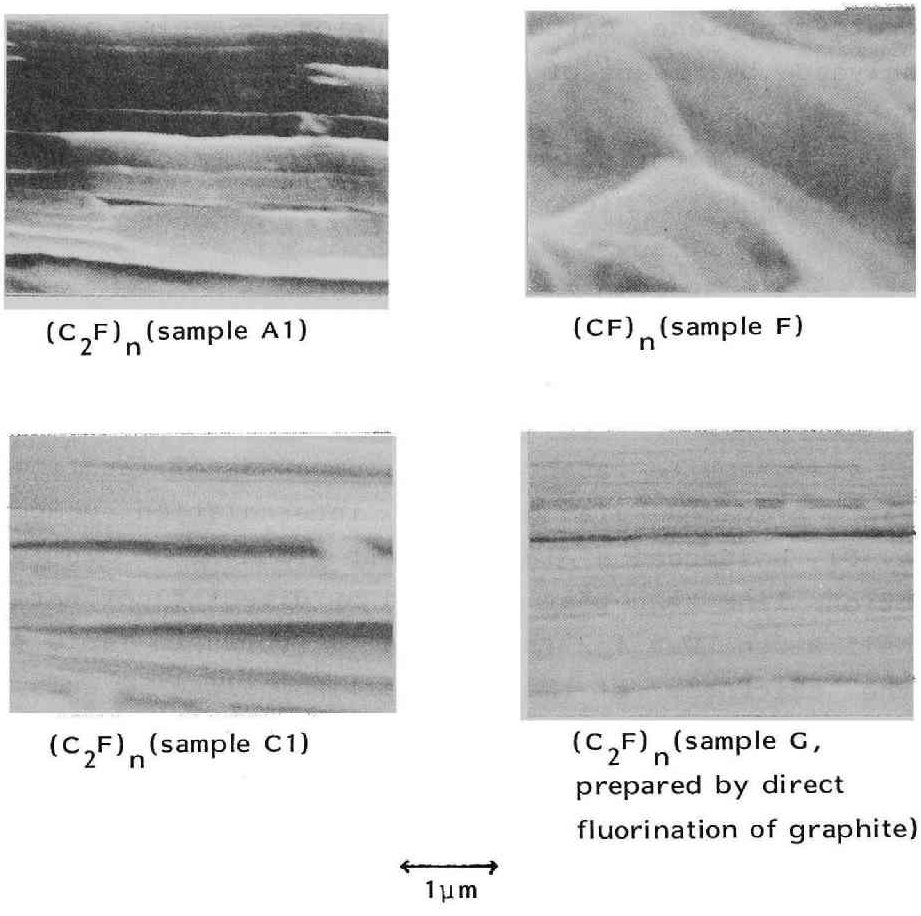

Fig. 4-1 SEM images of graphite fluorides prepared via graphite intercalation compounds

of the samples shown in Fig. 4-1 also indicate that $(CF)_n$ prepared by the present method(sample F) is remarkably exfoliated along the C axis compared with $(C_2F)_n$ prepared by the conventional method (sample G). The degree of exfoliation in $(C_2F)_n$'s (samples A1 and C1) was not large as that of $(CF)_n$.

Exfoliation of host graphite layers along the C axis occurs by deintercalation of fluorine species in the thermal decomposition process of the intercalation compound. Exfoliation of graphite increases the surface area and the

reaction rate with fluorine. As shown in Table 4-1, direct fluorination of natural graphite at 340-350°C needed several hundreds of hours(sample G), however, it was decreased to less than 100 h by this method (sample A1). Reaction rates were drastically increased at higher temperatures(samples B, C1, C2). Fluorination at relatively low temperatures increased the F/C ratio with increasing fluorination time(samples A1, A2 and D1, D2). However, unreacted graphite was not detected by X-ray diffraction measurement for samples A1 and D1, which were prepared by short-time fluorination compared with A2 and D2. Thus unreacted amorphous carbon which causes no coherent scattering of X-ray still exists in $(C_2F)_n$ prepared with the present method at a low temperature. $(CF)_n$ was produced by rapid decomposition of the intercalation compounds with a high rate of temperature increase, which achieved a larger expansion of graphite as shown in Fig. 4-1(sample F). Reaction time was decreased to be less than 30 min while the conventional method needed 18 hours when the natural graphite was used as a starting carbon. Only flaky natural graphite could be used as a starting carbon to prepare $(CF)_n$ by the present method because the decomposition to fluorocarbon gas occurred explosively when other carbons with lower crystallinities and smaller particle sizes were used.

Discharge curves of graphite fluorides by direct fluorination and via graphite intercalation compounds are shown in Fig's 4-2 and 4-3. CCV's and overpotentials of the prepared samples at 25% discharge are listed in Table 4-3. Both $(C_2F)_n$ and $(CF)_n$ prepared via graphite intercalation compound indicated higher discharge potentials than those prepared by direct fluorination of the same graphite at around the same temperature. In the case of $(C_2F)_n$, almost the same overpotentials around 0.9 V were observed for both, that is, the difference in discharge potentials

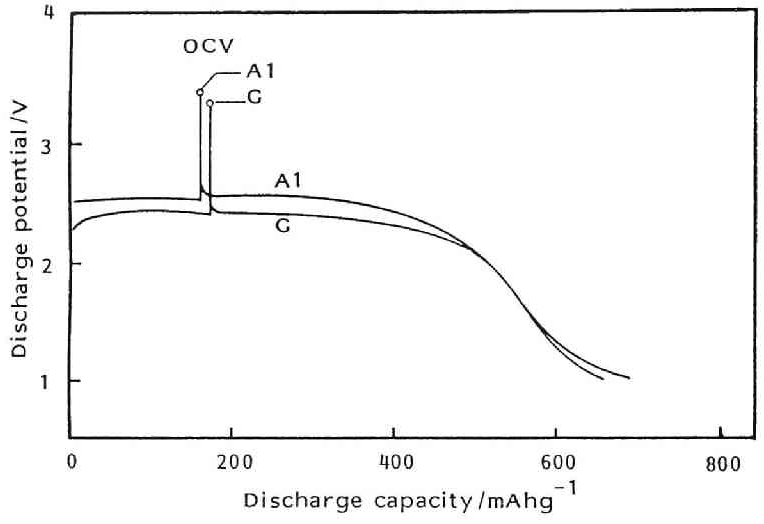

Fig. 4-2 Discharge characteristics of $(C_2F)_n$ prepared from natural graphite

A1: prepared from Madagascar natural graphite via GIC at 340°C
G : prepared from Madagascar natural graphite by direct fluorination at 350°C

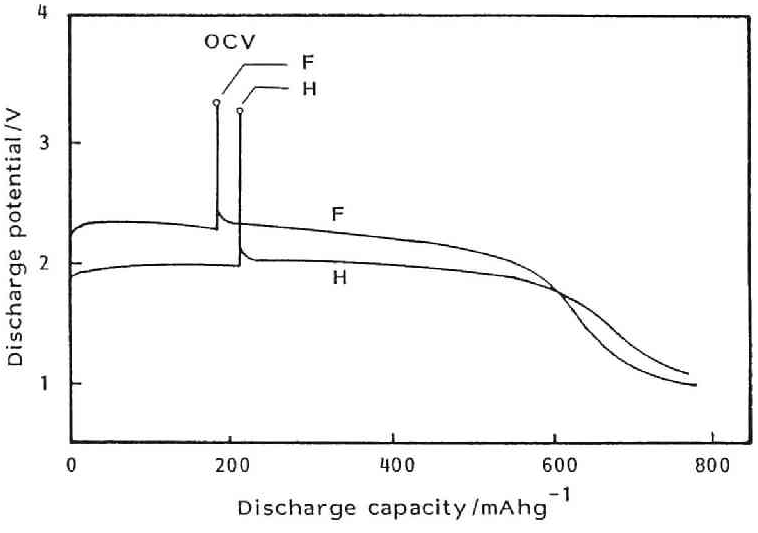

Fig. 4-3 Discharge characteristics of $(CF)_n$ prepared from natural graphite

F: prepared from Madagascar natural graphite via GIC at 350°C
H: prepared from Madagascar natural graphite by direct fluorination at 610°C

Table 4-3 Characteristics of graphite fluorides as cathodes

Sample	Starting material	Temp./°C	OCV[1]/V	CCV[2]/V	O.P.[3]/V
A1	Madagascar natural graphite(61-74 μm)	340	3.44	2.57	0.87
A2	Madagascar natural graphite(61-74 μm)	340	3.42	2.50	0.92
B	Madagascar natural graphite(61-74 μm)	390	3.36	2.47	0.89
C1	Madagascar natural graphite(61-74 μm)	440	3.32	2.38	0.94
C2	Madagascar natural graphite(61-74 μm)	430	3.34	2.37	0.97
D1	2800°C heat-treated petroleum coke	340	3.52	2.58	0.94
D2	2800°C heat-treated petroleum coke	340	3.45	2.55	0.90
E	2800°C heat-treated petroleum coke	430	3.40	2.51	0.89
F	Madagascar natural graphite(200-830 μm)	430	3.32	2.33	0.99
G	Madagascar natural graphite(61-74 μm)	350	3.30	2.41	0.89
H	Madagascar natural graphite(200-830 μm)	610	3.27	2.04	1.23

1) At 25% discharge.
2) At 25% discharge, vs. Li/Li^+, apparent current density of 0.50 $mAcm^{-2}$.
3) Overpotential, at 25% discharge, apparent current density of 0.50 $mAcm^{-2}$.

was almost equal to the difference in OCV's. However, the overpotential of $(CF)_n$ prepared via a graphite intercalation compound was less by 0.3 V than that prepared by direct fluorination, while OCV's of both were nearly the same. Discharge curves of $(C_2F)_n$'s prepared at various temperatures from natural graphite via graphite intercalation compound are shown in Fig. 4-4. As their overpotential

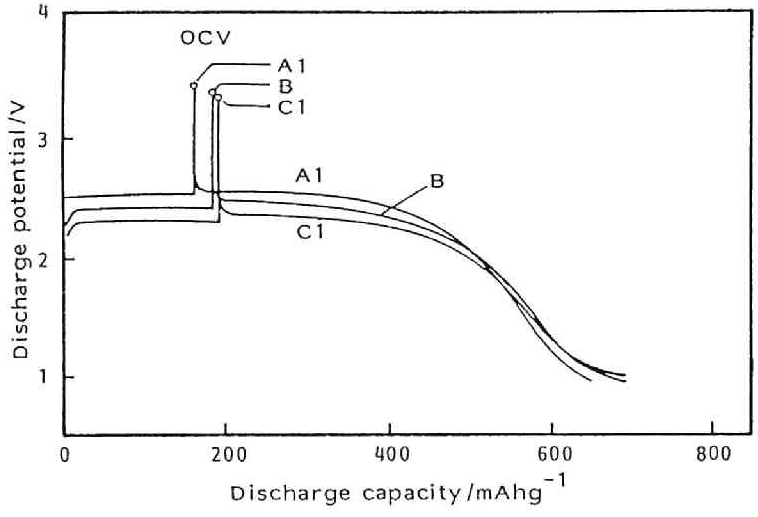

Fig. 4-4 Discharge characteristics of $(C_2F)_n$ prepared from Madagascar natural graphite via GIC
A1: at 340°C, B: at 390°C, C1: at 440°C

are nearly the same, the difference in CCV's arises from the difference in OCV's, which was increased with decreasing fluorination temperature.

$(C_2F)_n$ and $(CF)_n$ prepared by direct fluorination of natural graphite indicate the same OCV around 3.2-3.3 V vs lithium reference electrode in 1M $LiClO_4$-propylene carbonate solution as discussed in Chapter 1. On the other hand, higher OCV's are observed for graphite fluorides prepared from low-crystallized graphites at low temperatures. This would be due to the difference in the activities of the bulk fluorine species in graphite fluorides. In such graphite fluorides, the formation of a host carbon lattice by cleavage of the double bond of graphite is not completed, hence the covalent bond between carbon and fluorine atoms are weakened by distortion. This would cause the high OCV. The chemical bonding state of bulk fluorines with a carbon lattice can be detected by ^{19}F-NMR spectra. Generally two

peaks, broad and sharp, appear in the spectrum of graphite fluoride prepared at a low temperature. The concentrations of fluorine species corresponding to the sharp peak were less than a few percent of the bulk fluorine species from the peak intensity and line width. Moreover, the sharp peak was not observed in the spectrum of $(CF)_n$ fluorinated at 600°C, and even for $(C_2F)_n$, the peak intensity decreased as the heat treatment temperature increased, while OCV was almost unchanged as shown in Chapter 3. Consequently fluorine species which determine the OCV are ascribed to the bulk ones giving a broad peak in NMR spectra. The peak width was about 9.0 G and never changed by the heat treatment when the graphite fluoride was prepared from a highly graphitized carbon. $(C_2F)_n$ and $(CF)_n$ prepared at around 430-440°C with the present method (sample C1 and F) indicated the same OCV's and line widths in NMR spectra as those prepared by direct fluorination of a highly graphitized carbon. As shown in Table 4-4, however, the line width of wide line absorption decreased with decreasing fluorination temperature in $(C_2F)_n$ prepared via graphite intercalation compounds, which shows the increase in the activity of bulk fluorines.

Table 4-4 Temperature dependence of line width in ^{19}F-NMR spectra of $(C_2F)_n$ prepared via graphite intercalation compound

Sample[1)]	Fluorination temp/°C	Line width/Gauss	
		Broad line	Sharp line
A1	340	8.4	1.6
B	390	8.6	1.6
C1	440	9.0	1.6

1) Prepared from Madagascar natural graphite (61-74μm).

The overpotential of $(C_2F)_n$ was less by 0.3- 0.4 V than that of $(CF)_n$ at the current density of 0.5 $mAcm^{-2}$ when they were prepared from natural graphite by direct fluorination. Two factors were noted concerning the smaller overpotential of $(C_2F)_n$ as shown in Chapter 3. One is the smaller thickness of crystallite along the C axis. The discharge proceeds along with the intercalation of a large solvated lithium ion into graphite fluoride layers to form a thin diffusion layer of graphite intercalation compound. The diffusion resistance to expand the graphite fluoride layers to form lithium ion site decreases with decreasing the thickness of the crystallite along C axis. The other factor was the existence of non-covalently bonded fluorine species regarded as a type of defect which remained in the intercalated layers of $(C_2F)_n$. These fluorine species are weakly bonded to polynuclear aromatic carbon rings remaining in the graphite fluoride prepared at low temperatures, giving a sharp peak in the ^{19}F-NMR spectra mentioned above. On the discharge of graphite fluoride, they promote the phase separation of the diffusion layer to lithium fluoride, carbon and solvent molecules to decrease the thickness of the diffusion layer. As shown in Table 4-1, $(C_2F)_n$ prepared from natural graphite via graphite intercalation compounds (sample A1 and A2) possess the same half widths in (002) diffraction lines as that of $(C_2F)_n$ prepared by direct fluorination at nearly the same temperature(sample G). The concentrations of non-covalently bonded fluorine species are not very different among graphite fluorides prepared at temperatures of less than 400°C, which was suggested by NMR measurements. As shown in Table 4-3, the overpotentials of these $(C_2F)_n$'s prepared with the present method are around 0.9 V at the current density of 0.5 $mAcm^{-2}$. However, $(C_2F)_n$'s prepared at more than 400°C(sample C1 and C2) showed a slightly larger overpotential which was considered to be caused by the decrease in

concentration of non-covalently bonded fluorine. On the other hand, $(CF)_n$ (sample F) with a much smaller thickness of crystallite along the C axis was prepared by this method at a low temperature. Because of the fluorination at a low temperature, the concentration of non-covalently bonded fluorine was higher than in $(CF)_n$ prepared by direct fluorination at 610°C (sample H). These would be the reasons why the overpotential was less than that of $(CF)_n$ prepared at a higher temperature.

3-2 The effect of heat treatment on the discharge characteristics

The heat treatment conditions of $(C_2F)_n$ in fluorine atmosphere, variations in F/C ratios and half widths of (002) diffraction lines are shown in Table 4-2. No change in F/C ratio and X-ray diffraction pattern was observed by the heat treatment of $(C_2F)_n$ prepared by direct fluorination(sample G)(see Chapter 3). The same tendency was also observed in the $(C_2F)_n$'s prepared from natural graphite via graphite intercalation compound at a relatively high temperature(sample C2). $(C_2F)_n$'s prepared at lower temperatures, however, showed increase in F/C ratios by the heat treatment(sample A2 and D2). As mentioned in Chapter 3, decomposition and refluorination of graphite fluorides occurs by heat treatment at temperatures of more than 600°C. DTA and TG analyses indicated that the decomposition temperatures in nitrogen atmosphere were 580-650°C for the samples prepared from natural graphite. However, for $(C_2F)_n$ prepared from natural graphite(sample A2), a large increase in F/C ratio was observed by the heat treatment at lower temperatures than these without any change in the position of the (002) diffraction line. Hence, this increase of F/C ratio is due to the fluorination of unreacted carbon existing in the graphite fluorides prepared by the present method. Fluorination of this unreacted carbon

contributes to the increase of F/C ratio differently from $(C_2F)_n$ prepared by direct fluorination. However, in the case of $(C_2F)_n$ prepared from graphitized petroleum coke(sample D2), the increase in F/C ratio was attributed to the increase in $(CF)_n$ content, by decomposition and refluorination of $(C_2F)_n$ because the (002) diffraction line shifted to the higher angle as the heat treatment temperature increased and at last split to two peaks of $(CF)_n$ and $(C_2F)_n$ at 600°C.

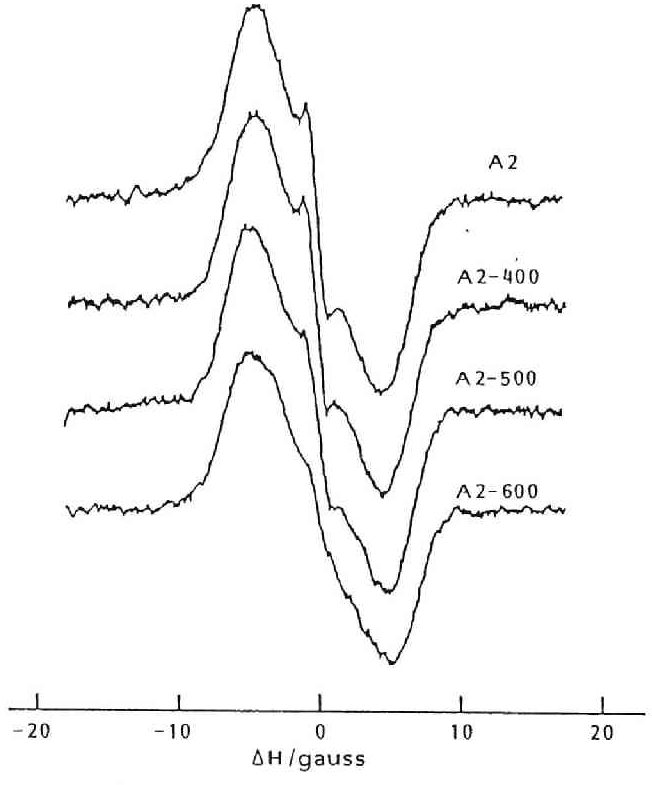

Fig. 4-5 ^{19}F-NMR spectra of heat-treated $(C_2F)_n$ prepared via GIC

A2: prepared from Madagascar natural graphite at 340°C

A2-400: A2 heat-treated at 400°C

A2-500: A2 heat-treated at 500°C

A2-600: A2 heat-treated at 600°C

The change in differential absorption lines of ^{19}F-NMR spectra by the heat treatment of $(C_2F)_n$ are shown in Fig.4-5. Two peaks were observed as mentioned above. As the heat treatment temperature increased, the broad peak widened and the intensity of the sharp peak decreased. The peak width of $(C_2F)_n$ prepared via graphite intercalation compound was less than 9.0 G before heat treatment, which was caused by a low temperature synthesis, then increased to 9.0 G with increasing heat treatment temperature. The decrease in intensity of the sharp peak was due to the formation of covalent bonds of weakly bonded fluorine with unreacted carbon remaining in $(C_2F)_n$ at high temperatures. Fig. 4-6 shows the changes in line widths and P value, which is an index of radical concentration in ESR

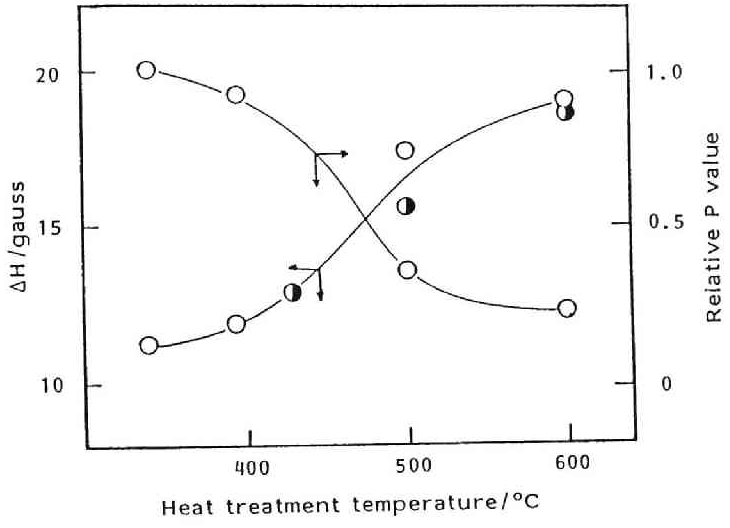

Fig. 4-6 Effect of heat treatment on the line width($\Delta H'$) and P value of ESR spectra of $(C_2F)_n$ prepared via GIC

○ : A2, A2-400, A2-500, A2-600

◑ : C2, C2-500, C2-600

P = (peak intensity) x $(\Delta H')^2/P_0$, P_0: P of A2.

spectra. The radicals were ascribed to that of carbon because the g value was 2.004 and did not change with the heat treatment as in the case of $(C_2F)_n$ prepared by direct fluorination. The increase of the line width and decrease of the P value are due to the localization of radicals by the double bond cleavage and by covalent bond formation of fluorine atoms with the unreacted carbon, that is, the decrease of radical concentration.

Figure 4-7 shows the changes in discharge characteristics of heat-treated $(C_2F)_n$, and Fig. 4-8 is the OCV and CCV dependence on the heat treatment temperature. The heat treatment in fluorine gas brought about the decrease of CCV, improvement of the flatness of discharge potential and increase of discharge capacity. OCV decreased by the heat treatment below 400°C but remained unchanged over 400°C. Overpotential was almost constant by 400°C and increased at higher temperatures. OCV decrease is considered to be caused by the change in the bonding of bulk fluorines which could be detected by NMR spectra discussed in Section 3-1. The increase of overpotential was caused by the decrease in concentration of weakly bonded fluorines which aid the lithium ion transfer in diffusion layers by accelerating the decomposition of the discharge product. The threshold temperature of 400°C was the same as in the case of $(C_2F)_n$ prepared by direct fluorination. The increase in discharge capacity coincides with the increase in F/C ratio by the heat treatment. The optimum temperature for heat treatment was around 450°C from the view points of discharge capacity, flatness of discharge potential and overpotential.

4. SUMMARY

(1) The preparations of graphite fluorides via ionic graphite intercalation compounds of fluorine markedly

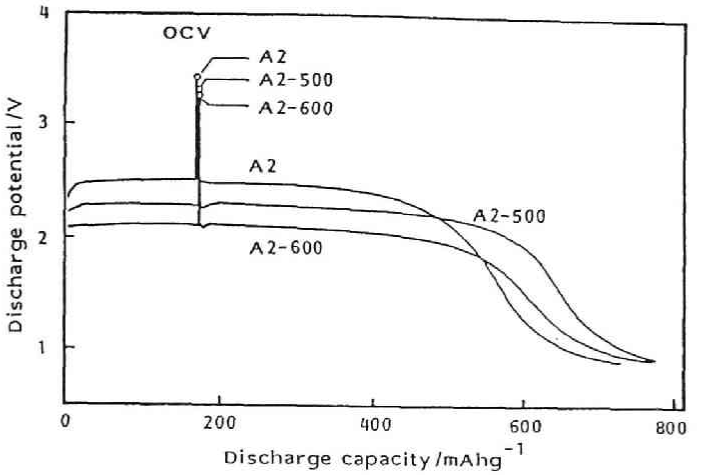

Fig. 4-7 Discharge characteristics of heat-treated $(C_2F)_n$

A2: prepared from Madagascar natural graphite via GIC at 340°C

A2-500: A2 heat-treated at 500°C

A2-600: A2 heat-treated at 600°C

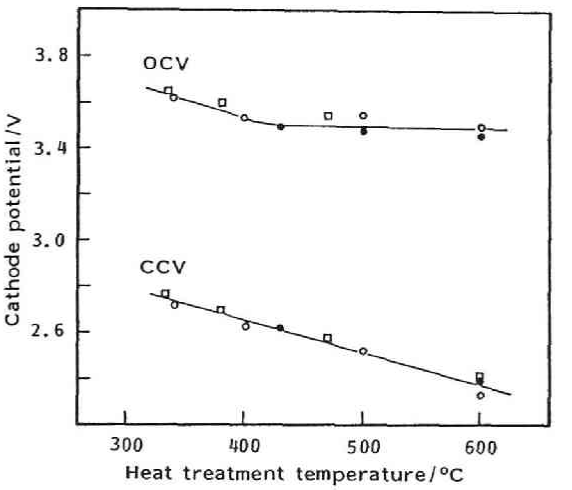

Fig. 4-8 OCV and CCV of heat-treated $(C_2F)_n$ prepared via GIC(at 25% discharge)

□: prepared from 2800°C-heat-treated petroleum coke at 340°C

○: prepared from Madagascar natural graphite at 340°C

●: prepared from Madagascar natural graphite at 430°C

decreased the reaction times compared with the direct fluorination method.

(2) OCV of $(C_2F)_n$ was higher by 0.2 V than that of the conventionally prepared one, however, overpotential was the same at the current density of 0.5 $mAcm^{-2}$. On the other hand, the same OCV and less overpotential by 0.3 V were observed for $(CF)_n$.

(3) The heat treatment of $(C_2F)_n$'s prepared by the present method in fluorine atmosphere at higher temperatures increased the discharge capacity and provided a more flat discharge potential. The optimum heat treatment temperature was around 450°C.

REFERENCE

[1] T. Nakajima, N. Kawaguchi and N. Watanabe, Carbon, 20, 287(1982).

Chapter 5

DISCHARGE CHARACTERISTICS OF $(CF)_n$ PREPARED FROM THE RESIDUAL CARBON OBTAINED BY THERMAL DECOMPOSITION OF GRAPHITE FLUORIDE AND OXIDE

1. INTRODUCTION

In the previous chapters, it has been revealed that the discharge characteristics are decisively influenced by the crystallinity and defect concentration of the graphite fluorides. These factors can be controlled by a careful choice of pristine carbon and reaction temperature. Since graphite fluorides are obtained only in the form of paracrystallite, the discharge performances of $(CF)_n$ and $(C_2F)_n$ are strongly dependent on their crystallinities. When comparison is made of $(CF)_n$ and $(C_2F)_n$ prepared from natural graphite, the difference in the discharge performances is summarized as follows:

1. Open circuit voltages of both are nearly the same, 3.2-3.3 V vs lithium reference electrode in 1M $LiClO_4$-propylene carbonate.
2. Overpotential of $(C_2F)_n$ electrode is smaller than that of $(CF)_n$. It is due to the facilitation of a solvated lithium ion transfer in the diffusion layer composed of discharge product, which arises from the higher defect concentration and smaller crystallite size along C axis in $(C_2F)_n$(see Chapter 2 and 3).
3. Discharge capacity of $(CF)_n$ is higher than that of $(C_2F)_n$. Theoretical discharge capacities are 860 and 700 $mAhg^{-1}$ for $(CF)_n$ and $(C_2F)_n$, respectively. Utilities of both are nearly the same, almost 100%, so

---

Submitted to J. Electrochem. Soc..

the difference arises from fluorine contents per unit weight.

Moreover, general characteristics of both $(CF)_n$ and $(C_2F)_n$ are as follows:

4. Graphite fluoride with a high crystallinity possesses a flat discharge potential and high utility. Discharge proceeds with the formation of the diffusion layer composed of a ternary graphite intercalation compound, which decomposes giving electroconductive carbon, lithium fluoride and solvent molecules. However, with decreasing crystallinity of graphite fluoride, the utility of fluorine decreases and the flatness of discharge potential becomes inferior. As shown in Chapter 1, when the real crystallite size of ab axis is very small like the sublimative graphite fluoride consisting of 5-19 fluorinated cyclohexane rings, the discharge of fluorine is difficult. This would be ascribed to that as the number of benzene rings in carbon layer decreases, namely as the crystallite size of ab axis decreases, carbon layer loses its electrical conductivity due to the localization of electrons. It is difficult to discharge a whole graphite fluoride having a small crystallite size along ab axis because of the difficulty in the recovery of electroconductive carbon.
5. The overpotential of graphite fluoride prepared from low graphitized carbon at a low temperature is smaller than that from highly graphitized carbon. Low graphitized carbon with a small crystallite size along C axis is easily fluorinated at a low temperature to give graphite fluoride with a high defect concentration and small crystallite size, both of which facilitate the diffusion of lithium ion.
6. Initial open circuit voltage of graphite fluoride

prepared from a low graphitized carbon at a low temperature is higher by 0.2-0.3 V than that from highly graphitized carbon. Graphite fluoride contains some amount of adsorbed fluorines, which gradually reacts with solvent of the electrolyte.

The required properties for a practical primary battery are a high and flat discharge potential, large capacity and high utility of active mass. Since the crystallinity of the pristine carbon is reflected in that of graphite fluoride, the crystallite size is a decisive factor for determining the discharge performance of graphite fluoride. As the growth of a crystallite by graphitization occurs simultaneously along both ab and C axis, it is very difficult to obtain a carbon composed of such crystallites that have a small size along C axis but some dimension in the direction of ab axis. So it is not so easy to achieve the simultaneous improvements of the above properties requested for a battery, in other words, to realize the flatness of discharge potential, high utility of active mass and low overpotential at the same time.

The aim of this chapter is to improve the discharge performance of graphite fluoride by the reform of the pristine carbon. The reform was made by thermal decomposition of graphite compounds with covalent bonds such as $(C_2F)_n$ and graphite oxide. The reformed carbons were refluorinated to form $(CF)_n$'s and their discharge behaviors were investigated.

2. EXPERIMENTAL

$(C_2F)_n$ was prepared by direct fluorination of Madagascar natural graphite under 1 atm of F_2 gas in a nickel reaction tube at 350°C for 3 weeks. Purities of carbon and fluorine were more than 98% and 99.4-99.7%,

respectively. $(C_2F)_n$ prepared was decomposed under argon gas at 600°C to produce the residual carbon. The decomposition temperature was determined by the aid of DTA and TG analyses.

Preparation of graphite oxide was made by the method previously reported(1). Madagascar natural graphite(10 g) and sodium nitrate(5 g, purity: 99.5%) was put in sulfuric acid(230 ml, purity: 95%), then potassium permanganate(30 g, purity: 99.3%) was added slowly to the solution stirred. After that, water was gradually poured in the solution for about ten minutes, during which temperature was raised up to 180°C by the heat of hydration. During this period, graphite oxide was formed at first and decomposition occurred successively. The residual carbon was washed in the funnel several tens of times until the neutralization of the filtrate, then dried under vacuum at 60°C for one day. The dried sample was heat-treated under vacuum at 400°C for 2 hours to remove the adsorbed oxygen.

Determination of lattice parameters and crystallite sizes of the residual carbons were performed by X-ray diffractometry(Cu-Kα).

Fluorination of the residual carbons were made at 300-600°C under F_2 gas flow. $(CF)_n$'s prepared were analysed by means of elemental analysis, X-ray diffractometry, SEM and ^{19}F-NMR.

Cell assembly and preparation of the electrodes were the same as shown in Chapter 1. All the experiments were performed at 25°C in the dry box of argon atmosphere.

3. RESULTS AND DISCUSSION

3-1 Preparation and structures of the residual carbons

From the DTA, thermal decomposition of $(C_2F)_n$ in argon atmosphere started at 480°C and finished at 600°C when the temperature was elevated by 5°C/min. TG indicated the

weight decrease of 61%. The residual carbon contained about 4wt% of fluorine, which was found to be adsorbed on the residual carbon according to the results of C_{1s} and F_{1s} ESCA spectra.

Determination of the detailed crystal structure of graphite oxide has not yet been succeeded. It would be due to non-stoichiometry and serious hygroscopicity of graphite oxide. However, a typical X-ray diffraction line around 0.6 nm(2) was observed when the terminal reaction temperature was kept at around 100°C. Decomposition of graphite oxide was completed at 180°C. The residual carbon dried in vacuo at 60°C contained about 20wt% of oxygen, which decreased to 12wt% by vacuuming at 400°C for two hours. The lattice parameter, $C_0(002)$ and half width of (002) diffraction line changed from 0.684 nm and 2.1° to 0.670 nm and 0.8°, respectively with this treatment. From the results obtained by X-ray diffractometry, almost all of oxygen remaining in the graphene layers were considered to be deintercalated by the first treatment, and oxygen species adsorbed or bound near the surface of the residual carbon, as O_2, H_2O, =O and -OH would have been partially eliminated by the second treatment.

Table 5-1 shows the lattice parameters and the size of the residual carbons with those of other typical pristine carbons as references. The crystallite sizes along ab and C axes are comparable in the case of general pristine carbons independently of whether they are large or small. The crystallite sizes remarkably decrease with the present methods compared with those of starting carbon. However, they have relatively large lengths along ab axis than C axis differently from other conventional carbons. It is reasonably ascribed to the anisotropic decomposition of graphite fluoride(3) and oxide.

Table 5-1 Lattice parameters and crystal sizes of the pristine carbons for preparation of graphite fluorides

Pristine carbons	$c_0(002)$ /nm	$L_c(002)$ /nm	$a_0(110)$ /nm	$L_a(110)$ /nm
Madagascar natural graphite	0.671	>100	0.246	>100
2800°C heat-treated petroleum coke	0.672	>100	0.246	>100
Non-heat-treated petroleum coke	0.690	3.6	---	2.8
Residual carbon via $(C_2F)_n$	0.675	4.6	0.246	28
Residual carbon via graphite oxide	0.670	14	0.246	44

3-2 Preparation and structure of $(CF)_n$ from the residual carbons

Table 5-2 shows the reaction condition and the results of elemental analysis and X-ray diffraction measurement of the graphite fluorides prepared from the residual carbons. The residual carbons were more easily fluorinated at lower temperatures and with a shorter reaction time of less than a few hours than the original natural graphite, giving $(CF)_n$. The anisotropic decomposition of graphite fluoride and oxide increases the surface area of residual carbon and its reaction rate with fluorine.

F/C ratios of $(CF)_n$'s fluorinated over 400°C were more than 0.9. With increasing fluorination temperature to 600°C, F/C ratio increased to about 1.1 corresponding to the value for conventional graphite fluoride. However, unreacted carbon was not detected by X-ray diffractometry even for $(CF)_n$ with the F/C ratio of 0.9. The color of $(CF)_n$ prepared at around 400°C was black or dark yellow. But the yellow color changed to black after several days. By the fluorination at higher temperatures, the color of $(CF)_n$ changed to white with increasing F/C ratio. Black color would be caused by the polynuclear aromatic carbon

Table 5-2 Synthetic conditions and analytical data of $(CF)_n$ prepared from the residual carbons

Pristine carbons	Fluorination temp./°C	F/C	d(002) /nm	β(002) /°	Type of $(C_xF)_n$
Residual carbon via $(C_2F)_n$	450	0.99	0.64	3.0	$(CF)_n$
	300	0.74	0.62	3.4	"
	600	1.11	0.58	1.4	"
Residual carbon via graphite oxide	500	0.94	0.63	3.2	"
	450	0.96	0.65	4.0	"
	400	0.90	0.70	4.6	"
	350	0.74	0.78	3.8	$(CF)_n$ + $(C_2F)_n$
	300	0.52	0.78	4.5	$(CF)_n$ + $(C_2F)_n$
Madagascar natural graphite	600	1.06	0.59	1.4	$(CF)_n$
	350	0.65	0.87	4.1	$(C_2F)_n$

rings remaining in $(CF)_n$ as unreacted part which is non-coherent to X ray, as in the case of $(C_2F)_n$ discussed in Chapter 3. As the fluorination temperature increases, unreacted part decreases hence the color changes to that of highly crystallized, white compound. The repeat distance along C axis, d(002) and half width of (002) diffraction line, β(002) decreased with increase of fluorination temperature. The carbon loss by the fluorination at 400-500°C was about 20%. At 600°C, carbon loss markedly increased to 70% and F/C ratio, d(002) and β(002) were the same as those of $(CF)_n$ prepared by direct fluorination of highly graphitized carbon. At this temperature, decomposition to fluorocarbons is so serious that only highly crystallized part is left as graphite fluoride.

The crystallite thickness along C axis of the residual carbon prepared via graphite oxide was about three times as that via $(C_2F)_n$, however, $(CF)_n$ prepared from the former had a larger half width of (002) diffraction line than the latter, in other words, the smaller crystallite size of C axis when fluorination was done at the same

temperature. As mentioned above, the residual carbon from graphite oxide contained a large amount of oxygen even after the heat treatment, but fluorinated residual carbon contained no oxygen. Hence the displacement of oxygen by fluorine must occur along with the fluorination, which would promote the strong exfoliation of the crystallite along C axis.

Figure 5-1 shows the SEM images of the residual carbons and $(CF)_n$'s prepared from them. The exfoliation along C axis is observed for the residual carbons. After the fluorination, $(CF)_n$'s obtained are markedly expanded along the same direction. Therefore the samples are spongy powder.

^{19}F-NMR spectra of the $(CF)_n$'s prepared are shown in Fig. 5-2 where two peaks, the broad and sharp, were observed. The broad peak corresponds to the bulk fluorine covalently bonded to carbon whose line width is about 9.0 G for both $(CF)_n$ and $(C_2F)_n$ prepared by direct fluorination of highly graphitized carbon. In case of the $(CF)_n$'s prepared from the residual carbon, the line width decreased by 1 G with decreasing fluorination temperature from 450 to 350°C. It would be caused by the distortion of the fluorine-carbon covalent bond due to the incompleteness of double bond cleavage of graphene layer at a low fluorination temperature. The narrow width line of about 1.5 G is ascribed to the fluorine species weakly bonded to polynuclear aromatic carbon rings which remain as unreacted part in graphite fluoride, as already discussed for $(C_2F)_n$ in Chapter 3. This fluorine species was not detected in $(CF)_n$ prepared by the conventional fluorination at high temperatures. This kind of defect would remain also in $(CF)_n$-type graphite fluoride prepared by such a low temperature fluorination. The overlaps of the narrow and broad lines were found for $(CF)_n$'s prepared via graphite oxide at relatively low temperatures because of the narrowing of the broad width line.

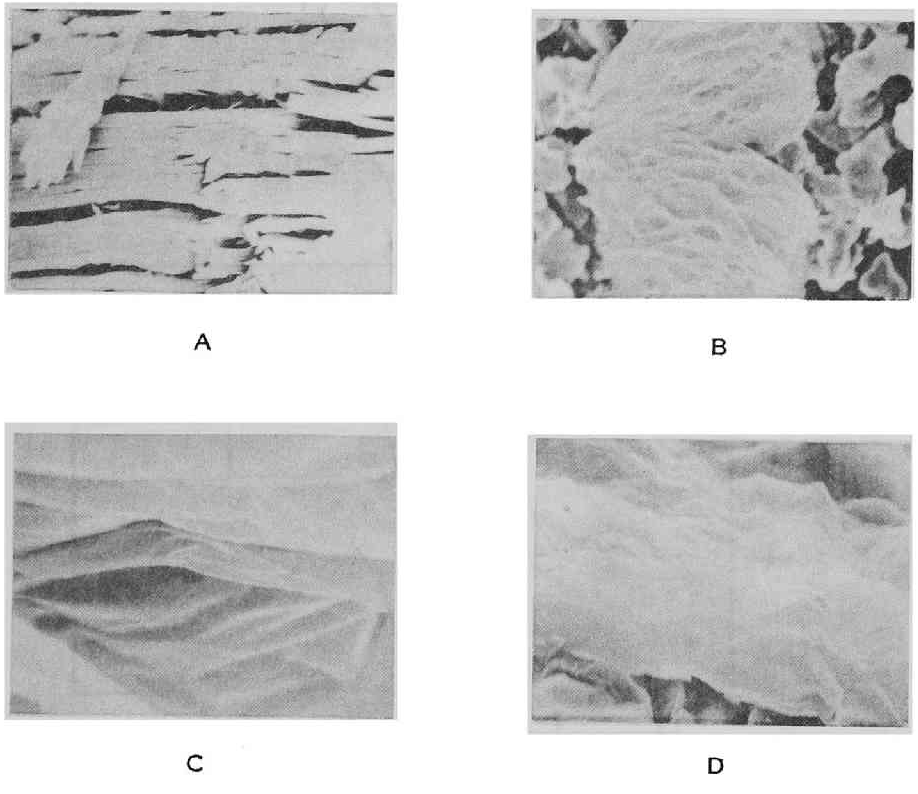

Fig. 5-1 SEM images of the residual carbons and $(CF)_n$'s

A: Residual carbon obtained by decomposition of $(C_2F)_n$

B: $(CF)_n$ obtained from A

C: Residual carbon obtained by decomposition of graphite oxide

D: $(CF)_n$ obtained from C

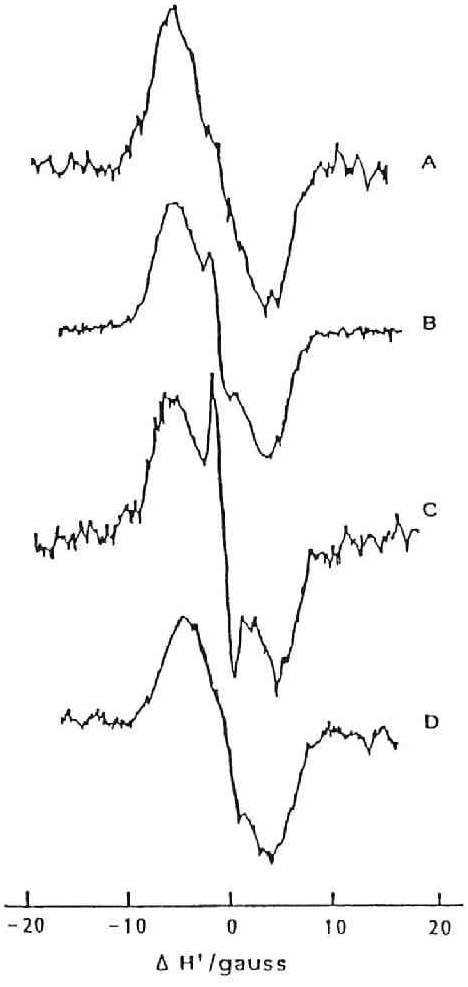

Fig. 5-2 ^{19}F-NMR spectra of graphite fluorides

A: $(CF)_n$ prepared from Madagascar natural graphite at 600°C

B: $(C_2F)_n$ prepared from Madagascar natural graphite at 350°C

C: $(CF)_n$ prepared from residual carbon via $(C_2F)_n$ at 450°C

D: $(CF)_n$ prepared from residual carbon via graphite oxide at 400°C

3-3 Discharge characteristics of $(CF)_n$'s prepared from the residual carbons

Typical discharge curves at a constant current density of 0.5 $mAcm^{-2}$ of $(CF)_n$'s prepared from the residual carbons at 400-450°C are shown in Fig. 5-3 in comparison with those of $(CF)_n$ and $(C_2F)_n$ prepared by direct fluorination of natural graphite. Higher discharge potentials than those of the conventional graphite fluorides were observed for $(CF)_n$'s prepared from both residual carbons. The flat discharge potential was also maintained during

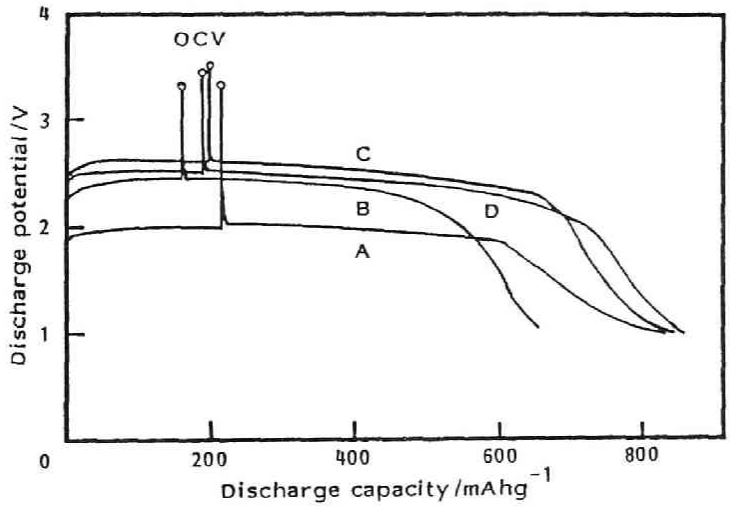

Fig. 5-3 Discharge curves of graphite fluoride cathodes (0.5 $mAcm^{-2}$, 1M $LiClO_4$-PC, 25°C)

A: $(CF)_n$ prepared from Madagascar natural graphite at 600°C

B: $(C_2F)_n$ prepared from Madagascar natural graphite at 350°C

C: $(CF)_n$ prepared from residual carbon via $(C_2F)_n$ at 450°C

D: $(CF)_n$ prepared from residual carbon via graphite oxide at 400°C

discharge as those of highly crystallized graphite fluorides.

Discharge characteristics of $(CF)_n$'s prepared via graphite oxide are summarized in Table 5-3. Change in discharge curves with fluorination temperature are shown in Fig. 5-4. As shown in Table 5-3, the open circuit voltages increased with decreasing fluorination temperature, which coincides with the narrowing of the line width of the broad line in ^{19}F-NMR spectra, suggesting the presence of the active bulk fluorine species. The overpotentials after 25% discharge at 0.5 $mAcm^{-2}$ were around 0.95 V for the $(CF)_n$'s fluorinated at 400-500°C. In this temperature range, the differences in the discharge potentials were mainly attributed to those in OCV's. Overpotentials were the same as that of $(C_2F)_n$ prepared by direct fluorination of natural graphite at around 350°C while these graphite fluorides were $(CF)_n$ type. Futhermore the flatness of discharge potential was comparable to that of highly graphitized ones and utility of the active mass was almost 100%.

The decrease in the overpotential is achieved by the low temperature fluorination of a carbon material with a thin crystallite along C axis. A small crystallite size of C axis of $(CF)_n$ facilitates the diffusion of a large solvated lithium ion which migrates making a site by expanding the $(CF)_n$ layers. Non-covalently bonded fluorine remaining in $(CF)_n$ which can be detected by ^{19}F-NMR as a sharp width line, also promotes the lithium ion transfer by accelerating the succeeding decomposition of the diffusion layer composed of the discharge product(see Chapter 3).

The crystallite size along ab axis, in other words, in the direction of lithium ion diffusion affects the flatness of discharge potential and utility of the cathode mass. The residual carbon had a larger dimension along ab axis than those of low grahitized carbon. Unfortunately the

Table 5-3 Discharge characteristics of graphite fluorides prepared from the residual carbons

Pristine carbons	Fluorination temp./°C	OCV* /V	CCV* /V	Over-pot.*/V	Disch. cap./mAhg^{-1}
Residual carbon via $(C_2F)_n$	450	3.49	2.55	0.94	850
	300	3.59	2.72	0.87	740
Residual carbon via graphite oxide	600	3.32	1.95	1.37	710
	500	3.32	2.35	0.97	840
	450	3.36	2.40	0.96	850
	400	3.45	2.51	0.94	850
	350	3.55	2.7	0.9	740
	300	3.62	2.9	0.7	600
Madagascar natural graphite	600	3.28	1.96	1.32	820
	350	3.30	2.41	0.89	690

* at 25% discharge, 0.5 mAcm^{-2}.

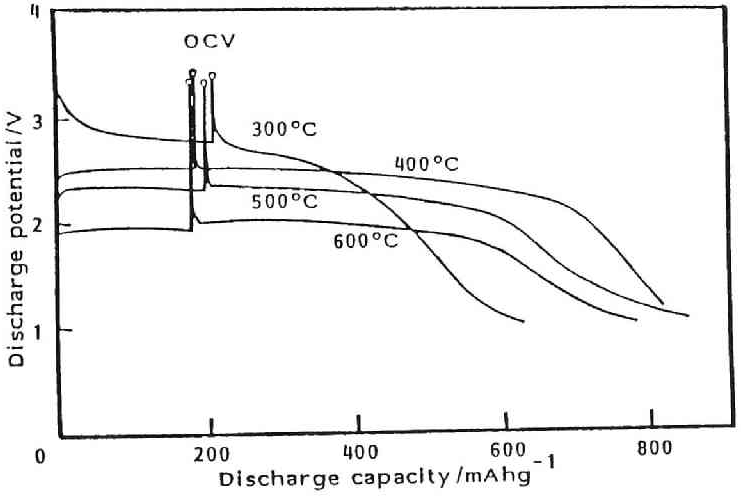

Fig. 5-4 Change in discharge curves of $(CF)_n$ prepared from the residual carbon via graphite oxide (0.5 mAcm^{-2}, 1M $LiClO_4$-PC, 25°C)

crystallite size along ab axis of $(CF)_n$ cannot be determined by X-ray diffractometry because of the overlap of the (100) diffraction line with others such as (101), which makes the determination of the peak width difficult. However, the anisotropy of the pristine carbon is reflected in that of $(CF)_n$ finally obtained though the expansion occurs along C axis by the intercalation of fluorine.

$(CF)_n$'s prepared at less than 400°C had higher discharge potentials, however, flatness of discharge potential was inferior and self discharge occurred at the beginning of the discharge. The discharge behavior of $(CF)_n$ prepared at 600°C was very much alike to that prepared by direct fluorination of highly graphitized carbon at the same temperature. As discussed in the Section 3-2, only highly crystallized part remained due to the decomposition reaction to gaseous fluorocarbons at this temperature. From the results above, appropriate temperature range for the preparation of $(CF)_n$ having the excellent performance is determined to be 400-500°C.

Galvanostatic polarization curves of graphite fluorides are shown in Fig. 5-5. The difference of the discharge potentials between $(CF)_n$ prepared from the residual carbon at 400°C and conventional $(C_2F)_n$ are around 0.2 V, which is attributed to the difference in the OCV's. The $(CF)_n$ prepared from the residual carbon indicated a higher discharge potential by 0.5 V than that prepared by the conventional method between the apparent current density of 0.01 - 1 $mAcm^{-2}$. Figure 5-6 shows the change of the discharge curve of $(CF)_n$ prepared from the residual carbon as a function of the current densities. When discharged at more than 1 $mAcm^{-2}$, utility of the cathode mass decreased from 100 %. However, discharge at the current density of 5 $mAcm^{-2}$ was possible for the $(CF)_n$ prepared with the present method while the conventional one failed to be discharged. $(CF)_n$ prepared from the residual carbon had

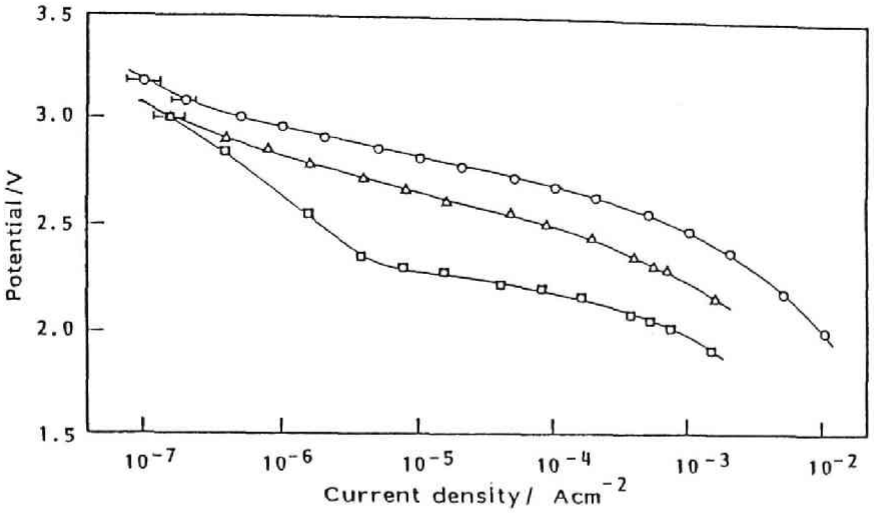

Fig. 5-5 Galvanostatic polarization curves of graphite fluorides at 25% discharge

○ : $(CF)_n$ prepared from residual carbon via graphite oxide at 400°C

△ : $(C_2F)_n$ prepared from Madagascar natural graphite at 350°C

□ : $(CF)_n$ prepared from Madagascar natural graphite at 600°C

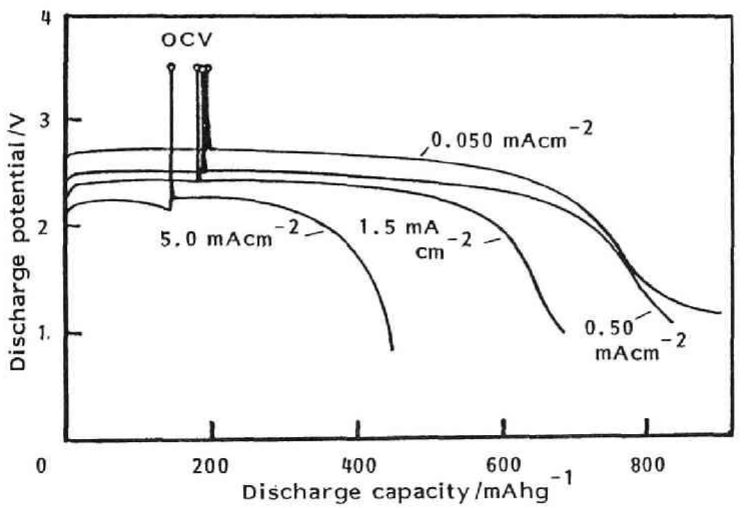

Fig. 5-6 Discharge curves of $(CF)_n$ prepared from residual carbon via graphite oxide at 400°C at various current densities(1M $LiClO_4$-PC, 25°C)

the energy density of 1900-2000 $Whkg^{-1}$ at the current density of 0.5 $mAcm^{-2}$. The increase in the energy density was 20-30% of the conventional $(CF)_n$.

4. SUMMARY

(1) The residual carbons obtained by thermal decomposition of graphite fluoride and oxide were found to be composed of such crystallinities having a smaller size along C axis than the dimension of ab axis. They were easily fluorinated giving $(CF)_n$'s at a relatively low temperature in a short time.

(2) $(CF)_n$'s prepared from the residual carbons had higher discharge potentials than the graphite fluorides prepared by direct fluorination. They have smaller thickness along C axis and higher defect concentration than the conventional ones by the low temperature fluorination of the residual carbon with a thinner stack along C axis, which provides a facilitation of lithium ion transfer in the diffusion layer.

(3) The utility of fluorine was almost 100%, and the flatness of discharge potential was also quite well when they were prepared at 400-500°C. The maximum increase of energy density achieved at the current density of 0.5 $mAcm^{-2}$ was about 30%.

REFERENCES

[1] W. S. Hummers, Jr. and R. E. Offeman, J. Am. Chem. Soc., 80, 1339(1958).

[2] W. Rudorff, Adv. Inorg. Chem., Radiochem., 1, 223 (1959).

[3] S. Koyama, Ph.D. Thesis in Kyoto University(1980).

Chapter 6

Properties of Initial Discharge Behaviour of Graphite Fluorides Decomposed Under Chlorine

1. INTRODUCTION

As mentioned in Chapter 1, graphite fluorides have layered structures in which fluorine atoms are covalently bonded to an array of trans-linked cyclohexane chairs of carbon atoms. It is having lost the aromatic nature of the host graphite, an essential difference from general intercalation compounds with planar graphite layers. Therefore graphite fluorides are electrical insulators.

On discharge the lithium ion is intercalated between the graphite fluoride layers to form a thin layer of graphite intercalation compound composed of carbon, fluorine and lithium with solvent molecules, which decomposes to lithium fluoride, graphite like carbon and solvent molecule as the discharge proceeds. At the beginning of discharge, a considerable drop in discharge potential is observed because insufficient formation of the conductive phase around the surface area of graphite fluoride particles has occured, so potential recovery needs from several to ca. 10% of discharge. Such behavior is undesirable from the viewpoint of the practical use of the battery, for example, the initial low potential is disadvantageous to determine the appropriate end point of the battery for instrument. To decrease the potential drop, the content of conductive additive must be increased in the cathode mixture in spite of the decrease in capacity of the cell. In this chapter, partial decomposition of graphite fluoride was effected in a chlorine atmosphere, and improvement in initial discharge

---

To be published in J. Appl. Electrochem..

behavior was investigated.

2. EXPERIMENTAL

Graphite fluorides were prepared by direct fluorination of Madagascar natural graphite(61-74 μm) under a fluorine atmosphere(1 atmosphere pressure). The reaction temperature and time were 600°C and 33 hrs for $(CF)_n$ and 350°C and 3 weeks for $(C_2F)_n$. Decomposition of the samples was performed under 1 atmosphere of chlorine in a silica tube. Between 0.5 and 1 g of the sample was put into the reaction tube, which was then evacuated and the temperature was increased up to that at which the partial decomposition of graphite fluoride was effected. After reaching the required temperature, the system was maintained for more than 10 hours in vacuum to adjust the temperature and to dry the sample. Chlorine gas was then introduced into the reaction tube after passing through calcium chloride at a pressure up to 1 atm. After 5 hours the reaction tube was cooled to the ambient temperature and residual chlorine gas was removed by argon flow. Elemental analysis, X-ray diffraction and ESCA measurements were performed on the samples.

Electrode preparation and cell assembly were the same as shown in Chapter 1. The electrolyte used was 1 molar $LiClO_4$-propylene carbonate solution(water content was less than 100 ppm). The cell was galvanostatically discharged at an apparent current density of 0.5 $mAcm^{-2}$ in a dry box filled with high purity argon.

3. RESULTS AND DISCUSSION

3-1 Decomposition of graphite fluorides under a chlorine atmosphere

Figure 6-1 shows the relation between the decomposition temperature and weight loss of the samples. In the case of

$(CF)_n$, the weight was almost unchanged below 400°C and a sudden weight decrease occurred at around 450°C. On the other hand, $(C_2F)_n$ gave little weight loss up to 300°C, but the sample weight gradually decreased with increasing temperature above 300°C. Figure 6-2 shows the change in X-ray diffraction powder pattern of $(C_2F)_n$. No change was observed for $(C_2F)_n$ decomposed under 300°C, however, the peak at around 26°, ascribed to the graphite (002) diffraction line, appeared on decomposition at 350°C. For $(CF)_n$, a large (002) graphite peak was first observed on decomposition at 450°C. Thus the residual carbon produced by this reaction posessed a graphite structure. The F/C ratios obtained from elemental analysis are shown as a function of weight decreases of graphite fluorides in Fig. 6-3. The solid lines in the figure indicate the F/C ratio calculated on the assumption that only the release of fluorine contributes to the weight loss of graphite fluoride. Hence the decrease of the F/C ratio is very large in comparison with other decomposition reactions of graphite fluoride in which fluorocarbons are formed(1-3). The experimental values agreed well with the calculated lines. Deviation from the theoretical lines is considered to be caused by weight increase due to chlorine species adsorbed on to the surface of the graphite fluoride particles which can be detected by elemental analysis and Cl_{2p} ESCA spectra. The amount of adsorbed chlorine was about 0.5wt% of the sample.

The F_{1s}, C_{1s} and Cl_{2p} ESCA spectra of partially decomposed $(C_2F)_n$ are shown in Fig. 6-4. With increasing temperature, the binding energy shifted to a lower position and the peak intensity decreased over 300°C in the F_{1s} spectra. This means that the covalent bond of fluorine around the surface of graphite fluoride changed to a weak bond such as is characteristic of chemical adsorption. The change of peak intensity coincides with the weight decrease results. In the C_{1s} ESCA spectra, the peak at 291 eV

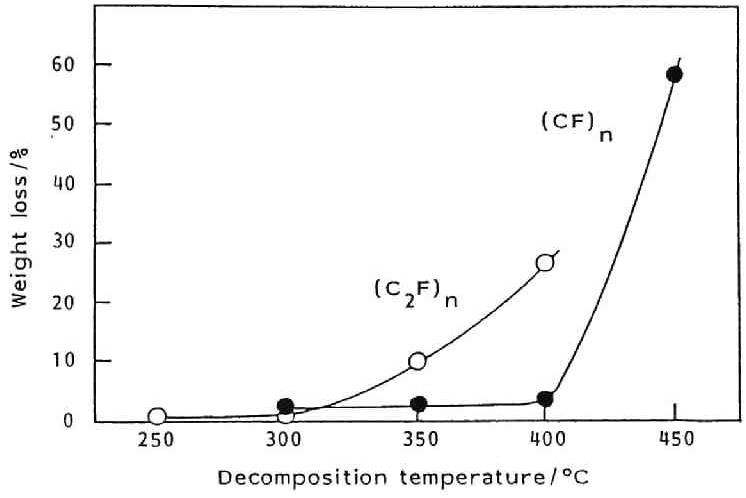

Fig. 6-1 Weight loss of graphite fluorides as a function decomposition temperature under Cl_2 atmosphere

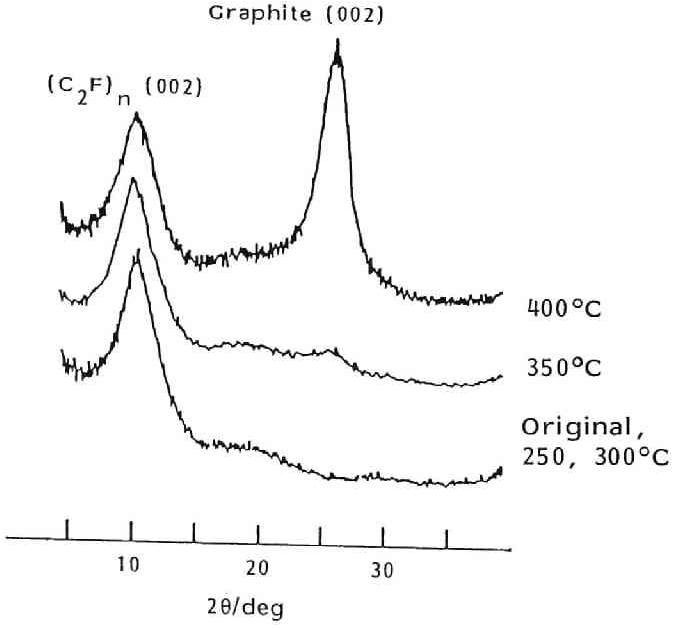

Fig. 6-2 X-ray diffraction pattern of $(C_2F)_n$ partially decomposed under a Cl_2 atmosphere

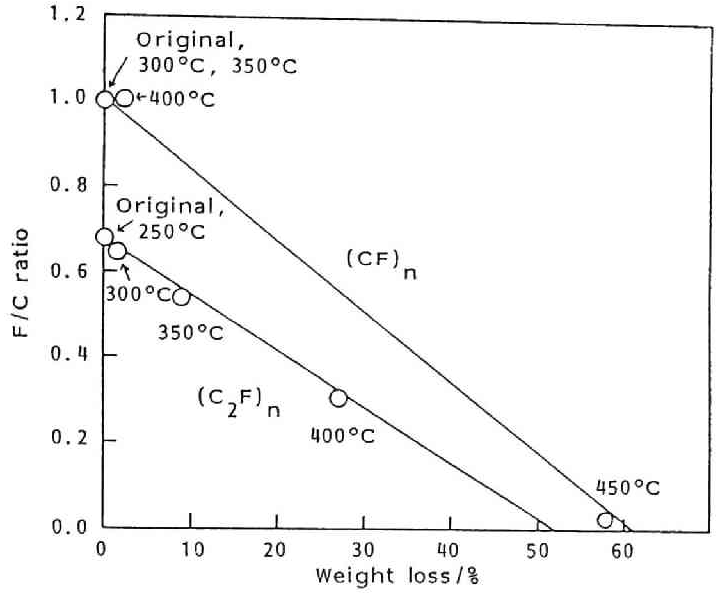

Fig. 6-3 Change in F/C ratio of graphite fluorides partially decomposed under Cl_2 atmosphere

corresponding to a covalent bond with fluorine shifted to a lower binding energy and the intensity decreased with increase of heat treatment temperature. On the other hand, a small peak at 284.3 eV corresponding to a carbon-carbon bond of graphite appeared for the sample decomposed at 300°C but the carbon phase could not be detected by X-ray diffractometry. This peak increased very much thereafter as the temperature increased. In Cl_{2p} spectra, three peaks were observed at and above 350°C. The Cl_{2p} spectrum includes two peaks, $Cl_{2p1/2}(L_{II})$ and $Cl_{2p3/2}(L_{III})$. The peaks at 202 and 200 eV correspond to a Cl-Cl covalent bond, and those at 200 and 198 eV are ascribed to a partially ionized chlorine species. The two peaks at 200 eV are overlapped. In the case of $(CF)_n$, the same phenomenon was found in ESCA spectra, but the change started at around 350°C.

Thus the decomposition of graphite fluorides in chlorine atmosphere is essentially different from that in

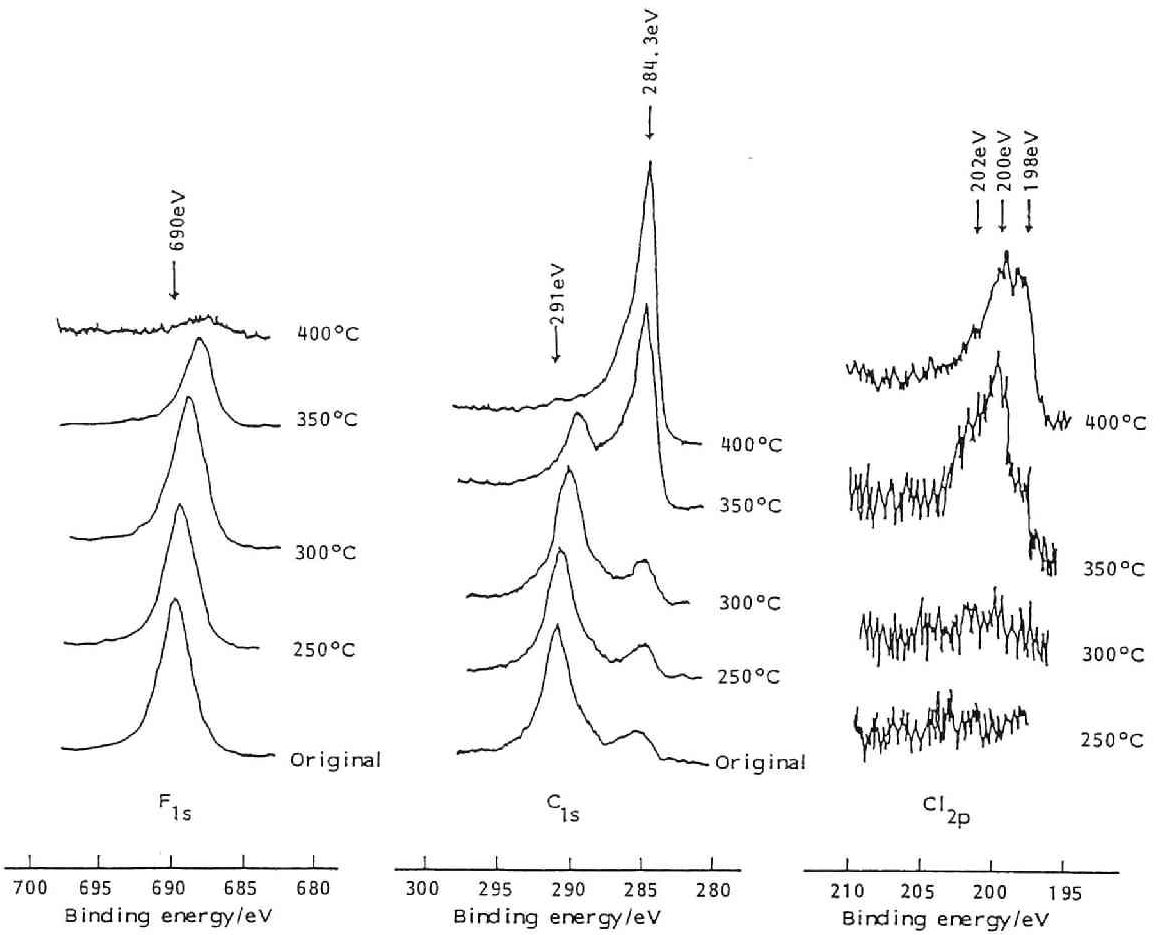

Fig. 6-4 ESCA spectra of $(C_2F)_n$ partially decomposed under a Cl_2 atmosphere

Table 6-1 Decomposition of graphite fluoride

	Atmosphere	F/C ratio of gas products F : C	Decomposition temp./°C
$(CF)_n$	vacuum[1,3]	2 : 1	620
	N_2[3]	2 : 1	560
	O_2[2,3]	1 : 1	<560
	Cl_2	1 : 0	≃400
$(C_2F)_n$	vacuum[3]	4 : 1	590
	Ar[3]	4 : 1	570
	Cl_2	1 : 0	≃300

other atmospheres previously reported(1-3). In Table 6-1, the decomposition of graphite fluorides in a chlorine atmosphere is compared with the decomposition in other atmospheres. The decomposition temperatures were much lower in a Cl_2 atmosphere and, moreover, no carbon consumption was found during the decomposition in this atmosphere. The results obtained suggests that graphite fluorides decompose to give interhalogen compounds such as ClF and ClF_3 in a chlorine atmosphere:

$$(C_xF)_n \xrightarrow{Cl_2} nxC(\text{graphite-like}) + ClF \text{ and/or } ClF_3$$

3-2 Effects of partial decomposition of graphite fluorides in a chlorine atmosphere on the discharge characteristics

If the reaction temperature and time are carefully controlled, the partial decomposition is expected to produce an electrically conductive carbon phase around the surface of the graphite fluoride particles without carbon loss. It has been found that an increase in overpotential is observed when heat treatment of $(C_2F)_n$ is carried out at more than 450°C in Chapter 3. Low temperature heat treatment in

a chlorine atmosphere can avoid such a problem.

Since graphite fluoride is an electrical insulator as a whole and the surface is covered with many CF_2 and CF_3 groups, addition of some electroconductive material and activation energy are needed to initiate the electrochemical reaction. For this reason, unnegligible potential drop is generally observed at the beginning of discharge. In the commercial battery, acetylene black is added to graphite fluoride by 5-20 wt% as the conductive additive. For the batteries containing acetylene black by 9 wt%, the initial potential drops range 130-150 mV and it takes from several to 8 hours to reach the flat discharge potential, which corresponds to ca. 10% discharge(4). Figure 6-5 shows the effects of partial decomposition under a chlorine atmosphere on the initial discharge characteristics of graphite fluoride electrodes. In the present study, graphite fluoride electrode was prepared by molding a 1:1:1 mixture in weight of graphite fluoride, acetylene black and polyethylene (binder) into a pellet, therefore, the initial potential drop was not so large as that of the commercial battery due to increase of the conductive additive. It is, however, obvious that the initial potential drop of non-heat-treated $(C_2F)_n$ disappeared when the sample was treated at 300°C. This can be ascribed to the increase of electrical conductivity through the carbon phase formed around the particle surface. However, some potential drop appeared again for the sample decomposed at 350°C, and a flat discharge potential was no longer observed for that decomposed at 400°C, possibly due to the difficulty in lithium ion transfer, caused by perfect covering with graphite-like carbon around the surface. Additionally, the decrease of the discharge capacity caused by fluorine loss was not negligible for the samples decomposed at a temperature higher than 350°C, being more than 10%. In the case of $(CF)_n$, the effects were not so marked as those with

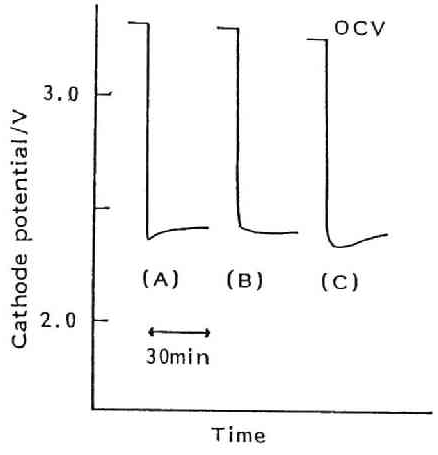

Fig. 6-5A Initial discharge characteristics of $(C_2F)_n$ partially decomposed under a Cl_2 atmosphere: (A) Original, (B) at 300°C, (C) at 350°C

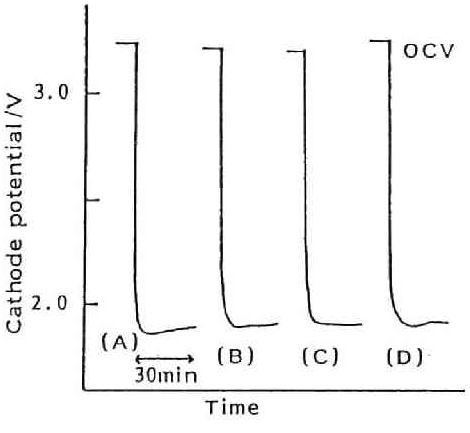

Fig. 6-5B Initial discharge characteristics of $(CF)_n$ partially decomposed under a Cl_2 atmosphere: (A) Original, (B) at 300°C (C) at 350°C, (D) at 400°C

$(C_2F)_n$, but the optimum decomposition temperature found was 350°C.

4. SUMMARY

(1) The main reaction of the decomposition of graphite fluorides under Cl_2 atmosphere is the carbon-fluorine bond rupture to form graphite-like carbon.
(2) The formation of a carbon film around the surface of graphite fluoride particles decreased the initial resistivity overpotential.
(3) The optimum decomposition temperatures were 300°C and 350°C for $(C_2F)_n$ and $(CF)_n$, respectively.

REFERENCES

[1] N. Watanabe, S. Koyama, H.Imoto, Bull. Chem. Soc. Jpn., 53, 2731(1980).
[2] N. Watanabe, T. Kawamura and S. Koyama, ibid., 53, 3100(1980).
[3] S. Koyama, Ph.D. Thesis, Kyoto University, Kyoto, Japan(1980).
[4] A. Morita, T. Iijima, T. Fujii and H. Ogawa, J. Power Source, 5, 111(1980).

CONCLUSION

The purpose of the present study is to investigate the reaction and kinetics of graphite fluoride electrode and effects of the structure on the discharge characteristics, and to develope new synthetic and reforming methods of graphite fluorides with better performances as a cathode material for primary lithium battery.

In Chapter 1, electrode reactions of two types of graphite fluorides, $(CF)_n$ and $(C_2F)_n$ were studied on the basis of electrochemical measurements. The effects of the electrolyte solvents on the electrode reaction were analysed using several kinds of organic solvents. A discharge model of cathode and formulation of the electrode potential were also presented.

(1) The discharge reaction of lithium-graphite fluoride is the formation of a thin ternary graphite intercalation compound(GIC) solvated with the solvent molecule, followed by the decompositive disproprotionation reaction.
(2) OCV's of lithium-$(CF)_n$ and $(C_2F)_n$ were nearly the same. OCV's increased with increasing solvation energy for Li^+ ion, which indicates the participation of the solvent molecules in the cell reaction.
(3) Cathode potential relative to lithium reference electrode varies with the product of activities of lithium and fluoride ions in GIC(I) phase.
(4) Graphite fluoride itself is an electrical insulator. Electron can be transported to the surface of graphite fluoride through the GIC(G) phase.

In Chapter 2, some kinetic parameters were obtained by transient techniques, and electrode kinetics of graphite fluorides were discussed.

(1)Cathode overpotentials of graphite fluoride electrodes is caused by the delay of lithium ion transfer in the thin diffusion layer composed of discharge products.
(2) The higher discharge potential of $(C_2F)_n$ electrode than that of $(CF)_n$ is due to the difference in the cathode overpotentials.
(3) Two factors must be taken into account for the difference in the cathode overpotentials between $(CF)_n$ and $(C_2F)_n$ electrodes. One is the difference in the diffusion coefficient, and the other is that in the thickness of diffusion layer. The contribution of the latter would be larger than the former.
(4) Activation energy for the lithium ion diffusion were 5.0 for $(CF)_n$ and 3.2 $kcalmol^{-1}$ for $(C_2F)_n$, respectively.

In Chapter 3, the relation between cathode overpotentials and crystallinity of $(CF)_n$ and $(C_2F)_n$ were investigated. The overpotentials are discussed on the basis of the results obtained by X-ray diffraction, ^{19}F-NMR and ESR measurements. Additionally, the effect of the solvents intercalated with a lithium ion on the discharge characteristics were discussed.

(1) The overpotential of $(CF)_n$ electrode decreased with increasing interlayer spacing and decreasing thickness of the crystallite along the C axis. The diffusion of a large solvated lithium ion needs expansion of host layers of graphite fluoride. A large interlayer spacing and small thickness of the crystallite along C axis facilitates the diffusion of lithium ion.
(2) The overpotential of $(C_2F)_n$ electrode depends on the defect concentration. Defects exist in the form of polynuclear aromatic carbon rings where fluorine species are non-covalently bonded. It promotes the decomposition of the

diffusion layer composed of a discharge product and decrease the thickness of diffusion layer. Defect concentration decreased by the heat treatment in fluorine atmosphere, which provided the overpotential increase.
(3) The higher discharge potential of $(C_2F)_n$ than that of $(CF)_n$ was mainly attributed to the effect of the defects contained in $(C_2F)_n$.
(4) Aprotic organic solvents by which a lithium ion is solvated also affects the overpotential. The larger the size of the solvent molecule, the larger the observed overpotential. It is due to difference in facility of lithium ion transfer in the diffusion layer.

In Chapter 4, the discharge characteristics of $(CF)_n$ and $(C_2F)_n$ prepared via ionic graphite intercalation compound of fluorine were investigated in comparison with those of graphite fluorides prepared by the direct fluorination of graphite.

(1) The preparations of graphite fluorides via ionic graphite intercalation compounds of fluorine markedly decreased the reaction times compared with the direct fluorination method.
(2) OCV of $(C_2F)_n$ was higher by 0.2 V than that of the conventionally prepared one, however, overpotential was the same at the current density of 0.5 $mAcm^{-2}$. On the other hand, the same OCV and less overpotential by 0.3 V were observed for $(CF)_n$.
(3) The heat treatment of $(C_2F)_n$'s prepared by the present method in fluorine atmosphere at higher temperatures increased the discharge capacity and provided a more flat discharge potential. The optimum heat treatment temperature was around 450°C.

In Chapter 5, improvement of the discharge performance

of graphite fluoride was made by the reform of the pristine carbon. The reform was made by thermal decomposition of graphite compounds with covalent bonds such as $(C_2F)_n$ and graphite oxide. The reformed carbons were refluorinated to form $(CF)_n$'s and their discharge behaviors were investigated.

(1) The residual carbons obtained by thermal decomposition of graphite fluoride and oxide were found to be composed of such crystallinities having a smaller size along C axis than the dimension of ab axis. They were easily fluorinated giving $(CF)_n$'s at a relatively low temperature in a short time.
(2) $(CF)_n$'s prepared from the residual carbons had higher discharge potentials than the graphite fluorides prepared by direct fluorination. They have smaller thickness along C axis and higher defect concentration than the conventional ones by the low temperature fluorination of the residual carbon with a thinner stack along C axis, which provides a facilitation of lithium ion transfer in the diffusion layer.
(3) The utility of fluorine was almost 100%, and the flatness of discharge potential was also quite well when they were prepared at 400-500°C. The maximum increase of energy density achieved at the current density of 0.5 $mAcm^{-2}$ was about 30%.

In Chapter 6, partial decomposition of graphite fluoride was effected in a chlorine atmosphere, and improvement in initial discharge behavior was investigated.

(1) The main reaction of the decomposition of graphite fluorides under Cl_2 atmosphere is the carbon-fluorine bond rupture to form graphite-like carbon.
(2) The formation of a carbon film around the surface of graphite fluoride particles decreased the initial resis-

tivity overpotential.

(3) The optimum decomposition temperatures were 300°C and 350°C for $(C_2F)_n$ and $(CF)_n$, respectively.